Search for supersymmetric particles in scenarios with a gravitino LSP and stau NLSP

DELPHI Collaboration

Abstract

Sleptons, neutralinos and charginos were searched for in the context of scenarios where the lightest supersymmetric particle is the gravitino. It was assumed that the stau is the next-to-lightest supersymmetric particle. Data collected with the DELPHI detector at a centre-of-mass energy near 189 GeV were analysed combining the methods developed in previous searches at lower energies. No evidence for the production of these supersymmetric particles was found. Hence, limits were derived at 95% confidence level.

arXiv:hep-ex/0103026v1 16 Mar 2001

P.Abreu[22], W.Adam[52], T.Adye[38], P.Adzic[12], Z.Albrecht[18], T.Alderweireld[2], G.D.Alekseev[17], R.Alemany[51], T.Allmendinger[18], P.P.Allport[23], S.Almehed[25], U.Amaldi[9,29], N.Amapane[47], S.Amato[49], E.G.Anassontzis[3], P.Andersson[46], A.Andreazza[9], S.Andringa[22], P.Antilogus[26], W-D.Apel[18], Y.Arnoud[9], B.Åsman[46], J-E.Augustin[26], A.Augustinus[9], P.Baillon[9], A.Ballestrero[47], P.Bambade[20], F.Barao[22], G.Barbiellini[48], R.Barbier[26], D.Y.Bardin[17], G.Barker[18], A.Baroncelli[40], M.Battaglia[16], M.Baubillier[24], K-H.Becks[54], M.Begalli[6], A.Behrmann[54], P.Beilliere[8], Yu.Belokopytov[9], K.Belous[44], N.C.Benekos[33], A.C.Benvenuti[5], C.Berat[15], M.Berggren[24], D.Bertrand[2], M.Besancon[41], M.S.Bilenky[17], M-A.Bizouard[20], D.Bloch[10], H.M.Blom[32], M.Bonesini[29], M.Boonekamp[41], P.S.L.Booth[23], G.Borisov[20], C.Bosio[43], O.Botner[50], E.Boudinov[32], B.Bouquet[20], C.Bourdarios[20], T.J.V.Bowcock[23], I.Boyko[17], I.Bozovic[12], M.Bozzo[14], M.Bracko[45], P.Branchini[40], R.A.Brenner[50], P.Bruckman[9], J-M.Brunet[8], L.Bugge[34], T.Buran[34], B.Buschbeck[52], P.Buschmann[54], S.Cabrera[51], M.Caccia[28], M.Calvi[29], T.Camporesi[9], V.Canale[39], F.Carena[9], L.Carroll[23], C.Caso[14], M.V.Castillo Gimenez[51], A.Cattai[9], F.R.Cavallo[5], V.Chabaud[9], M.Chapkin[44], Ph.Charpentier[9], P.Checchia[37], G.A.Chelkov[17], R.Chierici[47], P.Chliapnikov[9,44], P.Chochula[7], V.Chorowicz[26], J.Chudoba[31], K.Cieslik[19], P.Collins[9], R.Contri[14], E.Cortina[51], G.Cosme[20], F.Cossutti[9], M.Costa[51], H.B.Crawley[1], D.Crennell[38], S.Crepe[15], G.Crosetti[14], J.Cuevas Maestro[35], S.Czellar[16], M.Davenport[9], W.Da Silva[24], G.Della Ricca[48], P.Delpierre[27], N.Demaria[9], A.De Angelis[48], W.De Boer[18], C.De Clercq[2], B.De Lotto[48], A.De Min[37], L.De Paula[49], H.Dijkstra[9], L.Di Ciaccio[9,39], J.Dolbeau[8], K.Doroba[53], M.Dracos[10], J.Drees[54], M.Dris[33], A.Duperrin[26], J-D.Durand[9], G.Eigen[4], T.Ekelof[50], G.Ekspong[46], M.Ellert[50], M.Elsing[9], J-P.Engel[10], M.Espirito Santo[9], G.Fanourakis[12], D.Fassouliotis[12], J.Fayot[24], M.Feindt[18], A.Ferrer[51], E.Ferrer-Ribas[20], F.Ferro[14], S.Fichet[24], A.Firestone[1], U.Flagmeyer[54], H.Foeth[9], E.Fokitis[33], F.Fontanelli[14], B.Franek[38], A.G.Frodesen[4], R.Fruhwirth[52], F.Fulda-Quenzer[20], J.Fuster[51], A.Galloni[23], D.Gamba[47], S.Gamblin[20], M.Gandelman[49], C.Garcia[51], C.Gaspar[9], M.Gaspar[49], U.Gasparini[37], Ph.Gavillet[9], E.N.Gazis[33], D.Gele[10], T.Geralis[12], N.Ghodbane[26], I.Gil[51], F.Glege[54], R.Gokieli[9,53], B.Golob[9,45], G.Gomez-Ceballos[42], P.Goncalves[22], I.Gonzalez Caballero[42], G.Gopal[38], L.Gorn[1], Yu.Gouz[44], V.Gracco[14], J.Grahl[1], E.Graziani[40], P.Gris[41], G.Grosdidier[20], K.Grzelak[53], J.Guy[38], C.Haag[18], F.Hahn[9], S.Hahn[54], S.Haider[9], A.Hallgren[50], K.Hamacher[54], J.Hansen[34], F.J.Harris[36], F.Hauler[18], V.Hedberg[9,25], S.Heising[18], J.J.Hernandez[51], P.Herquet[2], H.Herr[9], T.L.Hessing[36], J.-M.Heuser[54], E.Higon[51], S-O.Holmgren[46], P.J.Holt[36], S.Hoorelbeke[2], M.Houlden[23], J.Hrubec[52], M.Huber[18], K.Huet[2], G.J.Hughes[23], K.Hultqvist[9,46], J.N.Jackson[23], R.Jacobsson[9], P.Jalocha[19], R.Janik[7], Ch.Jarlskog[25], G.Jarlskog[25], P.Jarry[41], B.Jean-Marie[20], D.Jeans[36], E.K.Johansson[46], P.Jonsson[26], C.Joram[9], P.Juillot[10], L.Jungermann[18], F.Kapusta[24], K.Karafasoulis[12], S.Katsanevas[26], E.C.Katsoufis[33], R.Keranen[18], G.Kernel[45], B.P.Kersevan[45], Yu.Khokhlov[44], B.A.Khomenko[17], N.N.Khovanski[17], A.Kiiskinen[16], B.King[23], A.Kinvig[23], N.J.Kjaer[9], O.Klapp[54], H.Klein[9], P.Kluit[32], P.Kokkinias[12], V.Kostioukhine[44], C.Kourkoumelis[3], O.Kouznetsov[17], M.Krammer[52], E.Kriznic[45], Z.Krumstein[17], P.Kubinec[7], J.Kurowska[53], K.Kurvinen[16], J.W.Lamsa[1], D.W.Lane[1], V.Lapin[44], J-P.Laugier[41], R.Lauhakangas[16], G.Leder[52], F.Ledroit[15], V.Lefebure[2], L.Leinonen[46], A.Leisos[12], R.Leitner[31], G.Lenzen[54], V.Lepeltier[20], T.Lesiak[19], M.Lethuillier[41], J.Libby[36], W.Liebig[54], D.Liko[9], A.Lipniacka[9,46], I.Lippi[37], B.Loerstad[25], J.G.Loken[36], J.H.Lopes[49], J.M.Lopez[42], R.Lopez-Fernandez[15], D.Loukas[12], P.Lutz[41], L.Lyons[36], J.MacNaughton[52], J.R.Mahon[6], A.Maio[22], A.Malek[54], T.G.M.Malmgren[46], S.Maltezos[33], V.Malychev[17], F.Mandl[52], J.Marco[42], R.Marco[42], B.Marechal[49], M.Margoni[37], J-C.Marin[9], C.Mariotti[9], A.Markou[12], C.Martinez-Rivero[20], S.Marti i Garcia[9], J.Masik[13], N.Mastroyiannopoulos[12], F.Matorras[42], C.Matteuzzi[29], G.Matthiae[39], F.Mazzucato[37], M.Mazzucato[37], M.Mc Cubbin[23], R.Mc Kay[1], R.Mc Nulty[23], G.Mc Pherson[23], C.Meroni[28], W.T.Meyer[1], A.Miagkov[44], E.Migliore[9], L.Mirabito[26], W.A.Mitaroff[52], U.Mjoernmark[25], T.Moa[46], M.Moch[18], R.Moeller[30], K.Moenig[9,11], M.R.Monge[14], D.Moraes[49], X.Moreau[24], P.Morettini[14], G.Morton[36], U.Mueller[54], K.Muenich[54], M.Mulders[32], C.Mulet-Marquis[15], R.Muresan[25], W.J.Murray[38], B.Muryn[19], G.Myatt[36], T.Myklebust[34], F.Naraghi[15], M.Nassiakou[12], F.L.Navarria[5], K.Nawrocki[53], P.Negri[29], N.Neufeld[9], R.Nicolaidou[41], B.S.Nielsen[30], P.Niezurawski[53], M.Nikolenko[10,17], V.Nomokonov[16], A.Nygren[25], V.Obraztsov[44], A.G.Olshevski[17], A.Onofre[22], R.Orava[16], G.Orazi[10], K.Osterberg[16], A.Ouraou[41], A.Oyanguren[51], M.Paganoni[29], S.Paiano[5], R.Pain[24], R.Paiva[22], J.Palacios[36], H.Palka[19], Th.D.Papadopoulou[9,33], L.Pape[9], C.Parkes[9], F.Parodi[14], U.Parzefall[23], A.Passeri[40], O.Passon[54], T.Pavel[25], M.Pegoraro[37], L.Peralta[22], M.Pernicka[52], A.Perrotta[5], C.Petridou[48], A.Petrolini[14], H.T.Phillips[38], F.Pierre[41], M.Pimenta[22], E.Piotto[28], T.Podobnik[45], M.E.Pol[6], G.Polok[19], P.Poropat[48], V.Pozdniakov[17], P.Privitera[39], N.Pukhaeva[17], A.Pullia[29], D.Radojicic[36], S.Ragazzi[29], H.Rahmani[33], J.Rames[13], P.N.Ratoff[21], A.L.Read[34], P.Rebecchi[9], N.G.Redaelli[29], M.Regler[52], J.Rehn[18], D.Reid[32], P.Reinertsen[4], R.Reinhardt[54], P.B.Renton[36], L.K.Resvanis[3], F.Richard[20], J.Ridky[13], G.Rinaudo[47], I.Ripp-Baudot[10], O.Rohne[34], A.Romero[47], P.Ronchese[37], E.I.Rosenberg[1], P.Rosinsky[7], P.Roudeau[20], T.Rovelli[5], Ch.Royon[41], V.Ruhlmann-Kleider[41], A.Ruiz[42], H.Saarikko[16], Y.Sacquin[41], A.Sadovsky[17], G.Sajot[15], J.Salt[51], D.Sampsonidis[12], M.Sannino[14], Ph.Schwemling[24], B.Schwering[54], U.Schwickerath[18], F.Scuri[48], P.Seager[21], Y.Sedykh[17], A.M.Segar[36], N.Seibert[18], R.Sekulin[38], R.C.Shellard[6], M.Siebel[54], L.Simard[41], F.Simonetto[37], A.N.Sisakian[17], G.Smadja[26], O.Smirnova[25], G.R.Smith[38], O.Solovianov[44], A.Sopczak[18], R.Sosnowski[53], T.Spassov[22], E.Spiriti[40], S.Squarcia[14], C.Stanescu[40], S.Stanic[45], M.Stanitzki[18], K.Stevenson[36], A.Stocchi[20], J.Strauss[52], R.Strub[10], B.Stugu[4], M.Szczekowski[53], M.Szeptycka[53], T.Tabarelli[29], A.Taffard[23], F.Tegenfeldt[50], F.Terranova[29], J.Thomas[36], J.Timmermans[32], N.Tinti[5], L.G.Tkatchev[17], M.Tobin[23], S.Todorova[9], A.Tomaradze[2], B.Tome[22], A.Tonazzo[9], L.Tortora[40], P.Tortosa[51], G.Transtromer[25], D.Treille[9], G.Tristram[8], M.Trochimczuk[53], C.Troncon[28], M-L.Turluer[41], I.A.Tyapkin[17], P.Tyapkin[25],

S.Tzamarias[12], O.Ullaland[9], V.Uvarov[44], G.Valenti[9,5], E.Vallazza[48], P.Van Dam[32], W.Van den Boeck[2], J.Van Eldik[9,32], A.Van Lysebetten[2], N.van Remortel[2], I.Van Vulpen[32], G.Vegni[28], L.Ventura[37], W.Venus[38,9], F.Verbeure[2], P.Verdier[26], M.Verlato[37], L.S.Vertogradov[17], V.Verzi[28], D.Vilanova[41], L.Vitale[48], E.Vlasov[44], A.S.Vodopyanov[17], G.Voulgaris[3], V.Vrba[13], H.Wahlen[54], C.Walck[46], A.J.Washbrook[23], C.Weiser[9], D.Wicke[9], J.H.Wickens[2], G.R.Wilkinson[36], M.Winter[10], M.Witek[19], G.Wolf[9], J.Yi[1], O.Yushchenko[44], A.Zalewska[19], P.Zalewski[53], D.Zavrtanik[45], E.Zevgolatakos[12], N.I.Zimin[17,25], A.Zintchenko[17], Ph.Zoller[10], G.C.Zucchelli[46], G.Zumerle[37]

[1]Department of Physics and Astronomy, Iowa State University, Ames IA 50011-3160, USA
[2]Physics Department, Univ. Instelling Antwerpen, Universiteitsplein 1, B-2610 Antwerpen, Belgium
 and IIHE, ULB-VUB, Pleinlaan 2, B-1050 Brussels, Belgium
 and Faculté des Sciences, Univ. de l'Etat Mons, Av. Maistriau 19, B-7000 Mons, Belgium
[3]Physics Laboratory, University of Athens, Solonos Str. 104, GR-10680 Athens, Greece
[4]Department of Physics, University of Bergen, Allégaten 55, NO-5007 Bergen, Norway
[5]Dipartimento di Fisica, Università di Bologna and INFN, Via Irnerio 46, IT-40126 Bologna, Italy
[6]Centro Brasileiro de Pesquisas Físicas, rua Xavier Sigaud 150, BR-22290 Rio de Janeiro, Brazil
 and Depto. de Física, Pont. Univ. Católica, C.P. 38071 BR-22453 Rio de Janeiro, Brazil
 and Inst. de Física, Univ. Estadual do Rio de Janeiro, rua São Francisco Xavier 524, Rio de Janeiro, Brazil
[7]Comenius University, Faculty of Mathematics and Physics, Mlynska Dolina, SK-84215 Bratislava, Slovakia
[8]Collège de France, Lab. de Physique Corpusculaire, IN2P3-CNRS, FR-75231 Paris Cedex 05, France
[9]CERN, CH-1211 Geneva 23, Switzerland
[10]Institut de Recherches Subatomiques, IN2P3 - CNRS/ULP - BP20, FR-67037 Strasbourg Cedex, France
[11]Now at DESY-Zeuthen, Platanenallee 6, D-15735 Zeuthen, Germany
[12]Institute of Nuclear Physics, N.C.S.R. Demokritos, P.O. Box 60228, GR-15310 Athens, Greece
[13]FZU, Inst. of Phys. of the C.A.S. High Energy Physics Division, Na Slovance 2, CZ-180 40, Praha 8, Czech Republic
[14]Dipartimento di Fisica, Università di Genova and INFN, Via Dodecaneso 33, IT-16146 Genova, Italy
[15]Institut des Sciences Nucléaires, IN2P3-CNRS, Université de Grenoble 1, FR-38026 Grenoble Cedex, France
[16]Helsinki Institute of Physics, HIP, P.O. Box 9, FI-00014 Helsinki, Finland
[17]Joint Institute for Nuclear Research, Dubna, Head Post Office, P.O. Box 79, RU-101 000 Moscow, Russian Federation
[18]Institut für Experimentelle Kernphysik, Universität Karlsruhe, Postfach 6980, DE-76128 Karlsruhe, Germany
[19]Institute of Nuclear Physics and University of Mining and Metalurgy, Ul. Kawiory 26a, PL-30055 Krakow, Poland
[20]Université de Paris-Sud, Lab. de l'Accélérateur Linéaire, IN2P3-CNRS, Bât. 200, FR-91405 Orsay Cedex, France
[21]School of Physics and Chemistry, University of Lancaster, Lancaster LA1 4YB, UK
[22]LIP, IST, FCUL - Av. Elias Garcia, 14-1°, PT-1000 Lisboa Codex, Portugal
[23]Department of Physics, University of Liverpool, P.O. Box 147, Liverpool L69 3BX, UK
[24]LPNHE, IN2P3-CNRS, Univ. Paris VI et VII, Tour 33 (RdC), 4 place Jussieu, FR-75252 Paris Cedex 05, France
[25]Department of Physics, University of Lund, Sölvegatan 14, SE-223 63 Lund, Sweden
[26]Université Claude Bernard de Lyon, IPNL, IN2P3-CNRS, FR-69622 Villeurbanne Cedex, France
[27]Univ. d'Aix - Marseille II - CPP, IN2P3-CNRS, FR-13288 Marseille Cedex 09, France
[28]Dipartimento di Fisica, Università di Milano and INFN-MILANO, Via Celoria 16, IT-20133 Milan, Italy
[29]Dipartimento di Fisica, Univ. di Milano-Bicocca and INFN-MILANO, Piazza delle Scienze 2, IT-20126 Milan, Italy
[30]Niels Bohr Institute, Blegdamsvej 17, DK-2100 Copenhagen Ø, Denmark
[31]IPNP of MFF, Charles Univ., Areal MFF, V Holesovickach 2, CZ-180 00, Praha 8, Czech Republic
[32]NIKHEF, Postbus 41882, NL-1009 DB Amsterdam, The Netherlands
[33]National Technical University, Physics Department, Zografou Campus, GR-15773 Athens, Greece
[34]Physics Department, University of Oslo, Blindern, NO-1000 Oslo 3, Norway
[35]Dpto. Fisica, Univ. Oviedo, Avda. Calvo Sotelo s/n, ES-33007 Oviedo, Spain
[36]Department of Physics, University of Oxford, Keble Road, Oxford OX1 3RH, UK
[37]Dipartimento di Fisica, Università di Padova and INFN, Via Marzolo 8, IT-35131 Padua, Italy
[38]Rutherford Appleton Laboratory, Chilton, Didcot OX11 OQX, UK
[39]Dipartimento di Fisica, Università di Roma II and INFN, Tor Vergata, IT-00173 Rome, Italy
[40]Dipartimento di Fisica, Università di Roma III and INFN, Via della Vasca Navale 84, IT-00146 Rome, Italy
[41]DAPNIA/Service de Physique des Particules, CEA-Saclay, FR-91191 Gif-sur-Yvette Cedex, France
[42]Instituto de Fisica de Cantabria (CSIC-UC), Avda. los Castros s/n, ES-39006 Santander, Spain
[43]Dipartimento di Fisica, Università degli Studi di Roma La Sapienza, Piazzale Aldo Moro 2, IT-00185 Rome, Italy
[44]Inst. for High Energy Physics, Serpukov P.O. Box 35, Protvino, (Moscow Region), Russian Federation
[45]J. Stefan Institute, Jamova 39, SI-1000 Ljubljana, Slovenia and Laboratory for Astroparticle Physics,
 Nova Gorica Polytechnic, Kostanjeviska 16a, SI-5000 Nova Gorica, Slovenia,
 and Department of Physics, University of Ljubljana, SI-1000 Ljubljana, Slovenia
[46]Fysikum, Stockholm University, Box 6730, SE-113 85 Stockholm, Sweden
[47]Dipartimento di Fisica Sperimentale, Università di Torino and INFN, Via P. Giuria 1, IT-10125 Turin, Italy
[48]Dipartimento di Fisica, Università di Trieste and INFN, Via A. Valerio 2, IT-34127 Trieste, Italy
 and Istituto di Fisica, Università di Udine, IT-33100 Udine, Italy
[49]Univ. Federal do Rio de Janeiro, C.P. 68528 Cidade Univ., Ilha do Fundão BR-21945-970 Rio de Janeiro, Brazil
[50]Department of Radiation Sciences, University of Uppsala, P.O. Box 535, SE-751 21 Uppsala, Sweden
[51]IFIC, Valencia-CSIC, and D.F.A.M.N., U. de Valencia, Avda. Dr. Moliner 50, ES-46100 Burjassot (Valencia), Spain
[52]Institut für Hochenergiephysik, Österr. Akad. d. Wissensch., Nikolsdorfergasse 18, AT-1050 Vienna, Austria
[53]Inst. Nuclear Studies and University of Warsaw, Ul. Hoza 69, PL-00681 Warsaw, Poland
[54]Fachbereich Physik, University of Wuppertal, Postfach 100 127, DE-42097 Wuppertal, Germany

1   Introduction

Supersymmetry (SUSY) may be broken at a scale below the grand-unification scale M_{GUT}, with the ordinary gauge interactions acting as the messengers of supersymmetry breaking [1,2]. In the corresponding models (GMSB models), the gravitino, $\tilde{G}$, turns out to be the lightest supersymmetric particle (LSP) and is expected to be almost massless. The next-to-lightest supersymmetric particle (NLSP) is therefore unstable and decays, under the assumption of R-parity conservation, into its ordinary matter partner and an invisible gravitino.

The number of generations of supersymmetry breaking messengers and the value of $\tan\beta$ usually determine which supersymmetric particle is the NLSP [3,4,5,6]. In the majority of the GMSB space, the NLSP is a slepton, $\tilde{l}$. Moreover, depending on magnitude of the mixing between $\tilde{\tau}_R$ and $\tilde{\tau}_L$, there exist two possible scenarios. If the mixing is large [1], $\tilde{\tau}_1$ is the NLSP, but if the mixing is negligible, $\tilde{\tau}_1$ is mainly right-handed [7] and almost mass degenerate with the other sleptons. In this case, the $\tilde{e}_R$ and $\tilde{\mu}_R$ three body decay ($\tilde{l} \to \tilde{\tau}_1 \tau l$ with $\tilde{\tau}_1 \to \tau \tilde{G}$), is very suppressed, and $\tilde{e}_R$ and $\tilde{\mu}_R$ decay directly into $l\tilde{G}$. This scenario is called $\tilde{l}$ co-NLSP. Searches for supersymmetric particles within both these scenarios are described in this article.

Due to the coupling of the NLSP to $\tilde{G}$, its mean decay length can range from μm to meters depending on the mass of the gravitino ($m_{\tilde{G}}$), or equivalently, on the scale of SUSY breaking, $\sqrt{F}$:

$$L = 1.76 \times 10^{-3} \sqrt{\left(\frac{E_{\tilde{l}}}{m_{\tilde{l}}}\right)^2 - 1} \left(\frac{m_{\tilde{l}}}{100\,\mathrm{GeV/c^2}}\right)^{-5} \left(\frac{m_{\tilde{G}}}{1\,\mathrm{eV/c^2}}\right)^2 \quad \mathrm{cm}, \qquad (1)$$

For example, for $m_{\tilde{G}} \lesssim 250$ eV ($\sqrt{F} \lesssim 1000$ TeV), the decay of the NLSP can take place within the detector. This range of $\sqrt{F}$ is in fact consistent with astrophysical and cosmological considerations [8,9].

The results of three searches are presented in this work. The first one looks for the production of $\tilde{\chi}_1^0$ pairs with either $\tilde{\chi}_1^0$ decaying to $\tilde{\tau}_1 \tau$ and $\tilde{\tau}_1$ then decaying promptly into $\tau\tilde{G}$, which is an update of the search presented in ref. [10], or $\tilde{\chi}_1^0$ decaying to $\tilde{l}l$ with $\mathrm{BR}(\tilde{\chi}_1^0 \to \tilde{l}l) = 1/3$ and $\tilde{l}$ promptly decaying into $l\tilde{G}$: $e^+e^- \to \tilde{\chi}_1^0\tilde{\chi}_1^0 \to \tilde{l}l\tilde{l}'l' \to l\tilde{G}ll'\tilde{G}l'$. These two modes represent the two extremes in the range of possible decays of the neutralino. In particular, a higgsino-like $\tilde{\chi}_1^0$ would decay only to $\tilde{\tau}_1\tau$ for all practical purposes since the higgsino component of the $\tilde{\chi}_1^0$ couples to $\tilde{l}$ through Yukawa couplings. On the other hand, the decays of a gaugino-like $\tilde{\chi}_1^0$ are regulated only by phase space considerations. Therefore, in the case of the $\tilde{\tau}_1$-NLSP scenario, neutralino pair production would mainly lead to a final state with four tau leptons and two gravitinos, while in the case of a co-NLSP scenario, the final signature would contain two pairs of leptons with possibly different flavour and two gravitinos.

The second search concerns $\tilde{l}$ pair production followed by the decays $\tilde{l} \to l\tilde{G}$ within the detector volume. The signature of such an event will be at least one track of a charged particle with a kink or a decay vertex when the $\tilde{l}$ decays inside the tracking devices. If the decay length is too short (small $m_{\tilde{G}}$) to allow for the reconstruction of the $\tilde{l}$ track, only the corresponding lepton or its decay products will be seen in the detector, and the search will then be based on track impact parameter. However, if the decay takes place outside the tracking devices (large $m_{\tilde{G}}$), the signature will be that of a heavy charged

---

[1]In GMSB models large mixing occurs generally in regions of $\tan\beta \geq 10$ or $|\mu| > 500$ GeV.

particle already studied by DELPHI [11]. For very light gravitinos the limits from the search for sleptons in gravity mediated (MSUGRA) models can be applied [12].

The third search looks for the pair-production of lightest charginos, $\tilde{\chi}_1^\pm$. Charginos, if produced in this context, would promptly decay through the channel $\tilde{\chi}_1^+ \to \tilde{\tau}_1^+ \nu_\tau$ [13]. The $\tilde{\tau}_1$ would then decay into $\tau\tilde{G}$, with non negligible mean lifetime. This search is divided into three sub-channels according to the mean lifetime of the stau as explained in the previous paragraph: two acoplanar leptons with missing energy, at least one track with large impact parameter or a kink, or at least one track corresponding to a very massive stable particle.

The data samples and event selections are respectively described in sections 2 and 3, while the results and a model dependent interpretation are presented in section 4.

2 Event sample and experimental procedure

All searches are based on data collected with the DELPHI detector during 1998 at a centre-of-mass energy of 189 GeV. The total integrated luminosity was 153.6 pb^{-1}. A detailed description of the DELPHI detector can be found in [14] and its performance in [15]. In all cases, the $\tilde{\tau}_1$-NLSP scenario searches are updates to similar searches carried out at lower centre-of-mass energies. All co-NLSP scenario searches are carried out at $\sqrt{s} = 189$ GeV.

To evaluate the signal efficiencies and Standard Model (SM) background contaminations, events were generated using different programs, all relying on JETSET 7.4 [16], tuned to LEP 1 data [17] for quark fragmentation. The program SUSYGEN [18] was used to generate the neutralino pair events and their subsequent decay products. In order to compute detection efficiencies, a total of 42000 events were generated with masses 67 GeV/$c^2 \leq m_{\tilde{\tau}_1} + 2$ GeV/$c^2 \leq m_{\tilde{\chi}_1^0} \leq \sqrt{s}/2$. A $\tilde{\tau}$ pair sample of 36000 events (subdivided in 36 samples) was produced with PYTHIA 5.7 [16] with staus having mean decay lengths from 0.25 to 200 cm and masses from m_τ to 90 GeV/c^2. Another sample of $\tilde{\tau}$ pair was produced with SUSYGEN for the small impact parameter search with $m_{\tilde{\tau}_1}$ from 7 to 80 GeV/c^2. Similar samples of smuons and selectrons were produced to study the sleptons co-NLSP scenario.

SUSYGEN was also used to generate the $\tilde{\chi}_1^\pm$ pair production samples and their decays. In order to compute detection efficiencies, a total of 45 samples of 500 events each were generated with $\tilde{G}$ masses of 1, 100 and 1000 eV/c^2, $m_{\tilde{\tau}_1} + 0.3$ GeV/$c^2 \leq m_{\tilde{\chi}_1^+} \leq \sqrt{s}/2$ and $m_{\tilde{\tau}_1} \geq 65$ GeV/c^2. Samples with smaller $\Delta m = m_{\tilde{\chi}_1^+} - m_{\tilde{\tau}_1}$ were not generated because in this region the $\tilde{\chi}_1^\pm$ does not decay mainly to $\tilde{\tau}_1$ and ν_τ but into W and $\tilde{G}$. The different background samples and event selections are described in references [19,20,11] for $m_{\tilde{G}} = 1$ and 1000 eV/c^2 respectively. For the case of $m_{\tilde{G}} = 100$ eV/c^2, the analysis is the same as the one used in the search for sleptons of this paper and consequently, the same sample of backgrounds is used.

The background process $e^+e^- \to q\bar{q}(n\gamma)$ was generated with PYTHIA 5.7, while DYMU3 [21] and KORALZ [22] were used for $\mu^+\mu^-(\gamma)$ and $\tau^+\tau^-(\gamma)$, respectively. The generator of reference [23] was used for $e^+e^- \to e^+e^-$ events.

Processes leading to four-fermion final states, $(Z/\gamma)(Z/\gamma)$, W^+W^-, $We\nu_e$ and Ze^+e^-, were also generated using PYTHIA. The calculation of the four-fermion background was verified using the program EXCALIBUR [24], which consistently takes into account all amplitudes leading to a given four-fermion final state.

Two-photon interactions leading to hadronic final states were generated using `TWOGAM` [25], separating the VDM, QPM and QCD components. The generators of Berends, Daverveldt and Kleiss [26] were used for the leptonic final states.

The cosmic radiation background was studied using the data collected before the beginning of the 1998 LEP run.

The generated signal and background events were passed through the detailed simulation [15] of the DELPHI detector and then processed with the same reconstruction and analysis programs used for real data.

3 Data selection

3.1 Neutralino pair production

The selection used in the search for the process $e^+e^- \rightarrow \tilde{\chi}_1^0\tilde{\chi}_1^0 \rightarrow \tilde{\tau}_1\tau\tilde{\tau}_1\tau \rightarrow \tau\tilde{G}\tau\tau\tilde{G}\tau$ has been described in [10]. A very similar selection was used in the general search for $e^+e^- \rightarrow \tilde{\chi}_1^0\tilde{\chi}_1^0 \rightarrow \tilde{l}l\tilde{l}'l' \rightarrow l\tilde{G}ll'\tilde{G}l'$ within the co-NLSP scenario, where $\mathrm{BR}(\tilde{\chi}_1^0 \rightarrow \tilde{l}l) = 1/3$ for each leptonic flavour. The main two differences between these two cases comes from the fact that the mean number of neutrinos carrying away undetected energy and momentum and the number of charged tracks per event is considerably bigger for the $\tilde{\tau}_1$-NLSP scenario. These differences can be appreciated in fig. 1, where the simulated missing energy normalized to the centre-of-mass energy and the number of charged tracks are represented for events with neutralinos weighing 82 GeV/c^2, and staus of 80 GeV/c^2, compared to events with same-mass neutralinos and degenerate sleptons of 80 GeV/c^2.

The pre-selection of events is common to both scenarios, and has been described in [10], together with the selection of the search for $\tilde{\chi}_1^0 \rightarrow \tilde{\tau}_1\tau$, which has not been changed for the present analysis. Only the details of the search $\tilde{\chi}_1^0 \rightarrow \tilde{l}l$ are presented in the following. Two sets of cuts were applied in order to reduce the $\gamma\gamma$ and $\mathrm{f\bar{f}}(\gamma)$ backgrounds and a third set of cuts to select events according to their topology:

1- Cuts against $\gamma\gamma$ backgrounds: the transverse energy, E_T, should be bigger than 4 GeV. The energy in a cone of 30° around the beam axis was further restricted to be less than 60% of the total visible energy to avoid possible bias from the Monte Carlo samples. The missing mass should be smaller than $0.88\sqrt{s}$. The momentum of the charged particle with largest momentum should be bigger than 8 GeV/c. The transverse missing momentum, p_T, should be bigger than 6 GeV/c. These cuts reduced the $\gamma\gamma$ background by a factor of the order of 40.

2- Cuts against $\mathrm{f\bar{f}}(\gamma)$ and 4-fermion backgrounds: the number of good tracks should be smaller than 7. The maximum thrust was further reduced from 0.99 to 0.95. Dividing each event into two jets with the Durham algorithm, its acoplanarity should be bigger than 8°. The missing mass of the events should be bigger than $0.2\sqrt{s}$. After these cuts, the $\mathrm{f\bar{f}}(\gamma)$ and 4-fermion backgrounds were reduced by a factor of the order of 30.

3- Cuts based on topology: signal events tend naturally to cluster into a 4-jet topology. When events are forced into a 4-jet configuration, all jets should be at least 18° away from the beam direction. When reduced by the jet algorithm into a 2-jet configuration, the charged particles belonging to each of these jets should be in a cone broader than 25°. Finally, the axes of each of the four jets should be separated from the others at least by 9°.

Figures 2 to 4 show some of the distributions relevant for these selection criteria. The discrepancy between data and simulation on the last two bins of figure 2-a is in a region of soft $\gamma\gamma$ events that is not relevant to the final results. Tables 1 and 2 show the effect of these cuts on the data, expected background and the signal for $m_{\tilde{\chi}_1^0} = 87$ GeV/c^2 and $m_{\tilde{\tau}_1} = 75$ GeV/c^2 for the cases $\tilde{\chi}_1^0 \to l\tilde{l}$ and $\tilde{\chi}_1^0 \to \tau\tilde{\tau}$ respectively.

One event was observed to pass the search for neutralino pair production in the $\tilde{\tau}_1$-NLSP scenario, with 1.16 ± 0.19 SM background events expected. Two events pass the search for neutralino pair production in the co-NLSP scenario, with 1.2 ± 0.30 SM background events expected. After these cuts, efficiencies between 27.0 and 40.7% were obtained for the signal events.

3.2   Slepton pair production

This section describes the update of the search for the process $e^+e^- \to \tilde{\tau}_1\tilde{\tau}_1 \to \tau\tilde{G}\tau\tilde{G}$ already described in [10,27]. An additional 153.6 pb^{-1} integrated luminosity collected at the centre-of-mass energy of 189 GeV has been analysed using the same procedure as for the data collected at 183 GeV and using the same values for the data selection cuts. The same selection cuts have been applied to the search for $\tilde{e}_{R^-}$ and $\tilde{\mu}_{R^-}$ pair production in the framework of $\tilde{l}$ co-NLSP scenario. Therefore, only results and efficiencies will be reported in this section, since the details of the selection criteria can be found in [10,27].

3.2.1   Search for secondary vertices

This analysis exploits a peculiarity of the $\tilde{l} \to l\tilde{G}$ topology in the case of intermediate gravitino masses (i.e. 0.5 eV/$c^2 \lesssim m_{\tilde{G}} \lesssim 200$ eV/c^2 as dictated by eq. 1), namely, one or two tracks coming from the interaction point and at least one of them with either a secondary vertex or a kink.

Rather loose preselection cuts were imposed on the events in order to suppress the low energy background (beam-gas, beam-wall, etc), $\gamma\gamma$, e^+e^- and hadronic events. The only cut that was changed with respect to the analysis at 183 GeV is the total electromagnetic energy required in the event. It was increased to $\sqrt{s}/2$ in order to improve the efficiency for selectrons. This did not increase noticeably the background contamination by Bhabha events. These preselection cuts left about 0.6% of the whole data sample. The events that survived the preselection cuts underwent the search for secondary vertices or kinks.

Fake decay vertices could be present amongst the reconstructed secondary vertices, being produced by particles interacting in the detector material or by radiated photons if the particle trajectory was reconstructed into two separated tracks. To eliminate these classes of events, additional requirements were imposed:

- to reject hadronic interactions, any reconstructed hadronic interaction (secondary vertices reconstructed in region where there is material) must be outside a cone of half angle 5° around the slepton direction;
- to reject segmented tracks, the angle between the tracks used to define a vertex had to be larger than 6°;
- to reject photon radiation in the case of τ clusters with only one track, there had to be no neutral particle in a 3° cone around the direction defined by the difference between the $\tilde{\tau}_1$ momentum and the momentum of the τ daughter calculated at the crossing point.

If no pair of tracks was found to survive these conditions, the event was rejected. Figure 5 shows the distribution of these three quantities. The distributions compare real data, expected Standard Model background simulation and simulated signal for $m_{\tilde{\tau}_1} = 60$ GeV/c^2 decaying with a mean decay length of 50 cm. The excess of data in the first bins of fig. 5-b is due to an underestimation in the simulation of mismatchings between the tracking devices.

One event in real data was found to satisfy all the conditions described above, while $1.18^{+0.63}_{-0.35}$ were expected from SM backgrounds. The event was compatible with a $\gamma\gamma \rightarrow \tau^+\tau^-$ with a hadronic interaction in the ID detector.

The vertex reconstruction procedure was sensitive to radial decay lengths, R, between 20 cm and 90 cm. Within this region a vertex was reconstructed with an efficiency of $\sim$52%. The VD (Vertex Detector) and the ID (Inner Detector) were needed to reconstruct the $\tilde{\tau}_1$ track and the TPC (Time Projection Chamber) to reconstruct the decay products. The shape of the efficiency distribution was essentially flat as a function of R, going down when the $\tilde{\tau}_1$ decayed near the outer surface of the TPC, due to inefficiencies in the reconstruction of the tracks coming from the desintegration products of the τ. Also, the sensitive region and the efficiency of the vertex reconstruction at 189 GeV was slightly lower than at 183 GeV due to the loss of tracks not reconstructed when their VD hits had no information in the z direction. Such tracks were not reconstructed for the 189 GeV run. However, some of the efficiency lost in the vertex search was recovered later by the search based on large impact parameter.

The search for vertices had an efficiency of the order of 46% for $\tilde{\tau}_1$ masses between 40 and 85 GeV/c^2 with a mean decay length of 50 cm. The efficiencies decreased near the kinematical limit due to a small boost that allowed for big angles to appear between the $\tilde{\tau}_1$ and the desintegration products of the τ. For $\tilde{\tau}_1$ masses below 40 GeV/c^2, the efficiency decreased gradually due to the cut that rejects segmented tracks. This happened because the resulting big boost causes the angle between $\tilde{\tau}_1$ and τ decay products to be very small.

As already said, the same selection criteria was applied to smuons and selectrons. The efficiency for selectrons decreased due to the preselection cut on total electromagnetic energy (lower than $0.5\sqrt{s}$) and was around 31% for $m_{\tilde{e}_R}$ between 40 to 85 GeV/c^2, while the smuon efficiency increased to 55% for the same mass range.

3.2.2 Large impact parameter search

To investigate a region of lower gravitino masses the previous search was extended to the case of sleptons with mean decay length between 0.25 cm and approximately 10 cm. In this case the $\tilde{l}$ track is not reconstructed and only the l (or the decay products in the case of $\tilde{\tau}$) is detected. The impact parameter search was only applied to those events accepted by the same general requirements as in the search for secondary vertices, and not selected by the vertex analysis. The same selection criteria described in references [10,27] were applied.

The efficiencies were derived for the different $\tilde{\tau}_1$ masses and decay lengths by applying the same selection to the simulated signal events. The maximum efficiency was 32% corresponding to a mean decay length of 2.5 cm. The efficiency decreased very fast for lower decay lengths due to the cut on minimum impact parameter. The efficiency at 189 GeV was slightly larger than at 183 GeV since some events not passing the secondary vertex selection were recovered in this search, as explained before. For longer decay lengths, the appearance of reconstructed $\tilde{\tau}_1$ tracks in combination with the cut on the maximum amount of charged particle tracks caused the efficiency to decrease smoothly.

This decrease is compensated by a rising efficiency in the search for secondary vertices. For masses above 30 GeV/c^2 no dependence on the $\tilde{\tau}_1$ mass was found far from the kinematic limit. However for lower masses the efficiency decreased and it was almost zero for a 5 GeV/c^2 $\tilde{\tau}_1$.

The same selection was applied to selectrons and smuons. For smuons the efficiency increased to 59% for a mean decay length of 2.5 cm and masses over 30 GeV/c^2 since the smuon has always one prong decay. For selectrons the efficiencies were almost the same as those for staus.

Trigger efficiencies were studied simulating the DELPHI trigger response to the events selected by the vertex search and by the large impact parameter analysis, and were found to be around 99%.

No events in the real data sample were selected with the above criteria, while $0.32^{+0.19}_{-0.10}$ were expected from SM backgrounds. The number of expected background events at $\sqrt{s} = 189$ GeV is shown in Table 3 for the combination of the vertex and large impact parameter searches.

3.2.3   Small impact parameter search

The large impact parameter search can be extended further down to mean decay lengths of around 0.1 cm. The same selection criteria described in reference [10] was applied. However, some extra selection was added in order to reduce background from detector noise or failure, cosmic radiation and $\tau\tau$ events.

Events with anomalous noise in the TPC were rejected requiring less than 20 charged particles (before track selection) and relative error of the measured momentum of the leading tracks (charged particles with largest momentum in each hemisphere) less than 50%. The cosmic muon rejection was improved by requiring that the leading tracks with impact parameters larger than 1 cm must be reconstructed in the TPC. To reduce the $\tau\tau$ background where one of the taus decays into a three prong topology (when the single track is not reconstructed), and also gamma conversions, any leading track must have at least other charged particle at an angular distance larger than 5°.

The efficiency of the search turned out not to depend on the $\tilde{\tau}_1$ mass for masses over 40 GeV/c^2, but rather on the $\tilde{\tau}_1$ decay length in the laboratory system. The maximum efficiency was $\sim 38\%$ for a mean decay length of ~ 2 cm, the efficiency dropped at small decay lengths ($\sim 15\%$ at 1 mm).

The same selection criteria were used to search for smuons. To search for selectrons, in order to increase efficiency, the cut $(E_1 + E_2) < 0.7E_{\text{beam}}$ (where E_1, E_2 are the electromagnetic energy deposits associated to the leading tracks) was not applied. The Bhabha events that survived the selection, when the previous rejection cut was not applied, were those where at least one of the electrons underwent a secondary interaction, thus acquiring a large impact parameter. However, it was found that in these cases the measured momentum of the electron was smaller than the electromagnetic energy deposition around the electron track. Therefore, the cut $(E_1/p_1 + E_2/p_2) < 2.2$ was used for the selectron search. The maximum efficiency reach for the smuon search was 43% and for the selectron search 35% at 2 cm mean decay length.

The number of events selected in data was 4, and $4.54^{+1.12}_{-0.57}$ events were expected from Standard Model background (see table 4). Two of the candidates had tracks with fitting problems and the other two events were compatible with Standard Model $\tau\tau$ events.

3.3   Chargino pair production

The analyses used to search for the lightest charginos varies according to the stau lifetime. Figures 5 and 6 illustrate the distributions of some of the main variables used in the analyses described respectively in section 3.2 (the stau decays with big impact parameter or producing a kink), and [19] (the stau decays at the main vertex). The plots show real data, expected Standard Model background, and a simulated signal of $m_{\tilde{\chi}_1^+} = 85$ GeV$/c^2$ and $m_{\tilde{\tau}_1^+} = 69$ GeV$/c^2$. For the three analyses described in section 2, Table 5 shows the range of efficiencies, the main components and the total amount of the expected background events, and the number of observed data events for each sample.

4   Results and interpretation

Since no evidence for a signal was found in the data, limits on the cross-section of sparticle pair production were derived. In what follows, the model described in reference [4] will be used in order to derive limits. This is a model which assumes radiatively broken electroweak symmetry and null trilinear couplings at the messenger scale. The SUSY soft parametes, gauge and Yukawa couplings are evolved between the electroweak scale (chosen to be m_t) and the messenger scale following the prescription of [28]. The masses of gauginos and sfermions at the messenger scale are calculated taking into account corrections arising from threshold effects. The corresponding parameter space was scanned as follows: $1 \leq n \leq 4$, 5 TeV $\leq \Lambda \leq 90$ TeV, $1.1 \leq M/\Lambda \leq 10^9$, $1.1 \leq \tan\beta \leq 50$, and $sign(\mu) = \pm 1$, where n is the number of messenger generations in the model, Λ is the ratio between the vacuum expectation values of the auxiliary component and the scalar component of the superfield and M is the messenger mass scale. The parameters $\tan\beta$ and μ are defined as for MSUGRA.

4.1   Neutralino pair production

Limits on the cross-section for neutralino pair production were derived in the two scenarios for each $(m_{\tilde{\chi}_1^0}, m_{\tilde{l}})$ combination. For the $\tilde{\tau}_1$-NLSP case, the combination took also into account the results from the LEP runs of 1996 and 1997 [10].

Figure 7-a shows the 95% C.L. upper limit for the $\tilde{\chi}_1^0$ pair production cross-section at $\sqrt{s} = 189$ GeV as a function of $m_{\tilde{\chi}_1^0}$ and $m_{\tilde{\tau}_1}$ after combining the results of the searches from $\sqrt{s} = 161$ up to 189 GeV with the likelihood ratio method [29], and scanning through the whole parameter space. Figure 7-b shows the 95% C.L. upper limit for the $\tilde{\chi}_1^0$ pair production cross-section at $\sqrt{s} = 189$ GeV as a function of $m_{\tilde{\chi}_1^0}$ and $m_{\tilde{l}_R}$. For different number of messenger generations, the ratios between production cross sections at different energies are bound to vary within certain limits. Figure 7 presents as an example the case of $n = 3$. For the other scenarios considered in this study ($n = 1$, 2 and 4), the maximum difference with respect to figure 7 is not bigger than 10%. This variation

4.2   Slepton pair production

Figure 8 shows the 95% C.L. upper limit on the slepton pair production cross-section at $\sqrt{s} = 189$ GeV after combining the results of the searches at $\sqrt{s} = 130$-189 GeV with the likelihood ratio method [29]. The results are presented in the $(m_{\tilde{G}}, m_{\tilde{l}})$ plane combining the two impact parameter searches, the secondary vertex analysis and the stable heavy

lepton search [11]. In particular, figure 8-a shows that the minimum upper limits achieved for a given $\tilde{\tau}_1$ were around 0.05-0.10 pb depending on $m_{\tilde{G}}$. For $m_{\tilde{G}} > 9$ eV/c^2 and a 80 GeV/c^2 $\tilde{\tau}_1$, a 0.10 pb limit was obtained. Figures 8-b and -c show the corresponding upper limit for $\tilde{\mu}_R$- and $\tilde{e}_R$ pair production cross-sections. Assuming mass degeneracy of the three supersymmetric particles, $\tilde{\tau}_1$, $\tilde{e}_R$ and $\tilde{\mu}_R$, figure 8-d shows the 95% C.L. upper limit for the $\tilde{l}_R$ pair production cross-section.

4.3   Chargino pair production

Limits on the production cross-section for chargino pairs were derived for each $(m_{\tilde{G}},m_{\tilde{\tau}_1},m_{\tilde{\chi}_1^+})$ combination. Figure 9 shows the 95% C.L. upper limit on the chargino pair production cross-section at $\sqrt{s} = 189$ GeV as a function of $m_{\tilde{\chi}_1^+}$ and $m_{\tilde{\tau}_1}$ after combining the results of the searches at $\sqrt{s} = 183$ and 189 GeV with the maximum likelihood ratio method [29] for $\Delta m \geq 0.3$ GeV/c^2 and $m_{\tilde{G}} = 1$, 100 and 1000 eV/c^2. These limits, which directly reflect the efficiencies of the applied selections, can be understood as follows:

$m_{\tilde{G}} = 1$ eV/c^2:	The efficiency of this analysis depends mainly on the mass of the chargino. To smaller chargino masses correspond bigger event missing energies, and bigger efficiencies.
$m_{\tilde{G}} = 100$ eV/c^2:	The map of efficiencies is the result of the convolution of two factors. First, larger stau masses imply a smaller lifetime, and hence a smaller efficiency. Second, a larger chargino mass leads to smaller stau momenta, and to smaller decay lengths.
$m_{\tilde{G}} = 1000$ eV/c^2:	In this case, the map of efficiencies is mainly affected by the momentum of the stau, because the method used to identify heavy stable particles relies on the lack of Cherenkov radiation in DELPHI's RICH detectors. To remove SM backgrounds, low momentum particles are removed, thus reducing the efficiency for higher chargino masses, especially in the region of small Δm.

4.4   Interpretation

4.4.1   Neutralino pair production

Given the aforementioned limits for the production cross-section, some sectors of the $(m_{\tilde{\chi}_1^0}, m_{\tilde{l}})$ space can be excluded. In order to achieve the maximum sensitivity, the results from two other analyses are taken into account. The first is the search for slepton pair production in the context of gravity mediated SUSY breaking models [12]. In the case where the MSUGRA $\tilde{\chi}_1^0$ is massless, the kinematics corresponds to the case of $\tilde{l}$ decaying into a lepton and a gravitino. The second is the search for lightest neutralino pair production in the region of the mass space where $\tilde{\chi}_1^0$ is the NLSP [30] (the region above the diagonal line in fig. 10, i.e. $m_{\tilde{\tau}} > m_{\tilde{\chi}_1^0}$). Within this zone, the neutralino decays into a gravitino and a photon.

As an illustration, fig. 10 presents the 95% C.L. excluded areas for $m_{\tilde{G}} < 1$ eV/c^2 in the $m_{\tilde{\chi}_1^0}$ vs. $m_{\tilde{l}_R}$ plane for the co-NLSP case. The positive-slope dashed area is excluded by this analysis. The resulting 95% C.L. lower limit for the mass of the lightest neutralino is 82.5 GeV/c^2. The negative-slope dashed area is excluded by the analysis searching for neutralino pair production followed by the decay $\tilde{\chi}_1^0 \to \tilde{G}\gamma$. The point-hatched area is excluded by the direct search for slepton pair production within MSUGRA scenarios [12].

Table 6 shows the 95 % C.L. lower limits on the mass of the lightest neutralino within the two scenarios for different n.

4.4.2 Slepton pair production

The $\tilde{\tau}_1$ pair production cross-section depends on the mixing in the stau sector. Therefore, in order to put limits to the $\tilde{\tau}_1$ mass the mixing angle has to be fixed. The results presented here corresponds to two cases within the $\tilde{\tau}_1$-NLSP scenario. In the first case, it is assumed that there is no mixing between the $\tilde{\tau}_R$ and $\tilde{\tau}_L$. Thus, $\tilde{\tau}_1$ is a pure right-handed state (figure 11-a). The second case (figure 11-b), corresponds to a mixing angle which gives the minimum $\tilde{\tau}_1$ pair production cross-section, while at the same time holds $m_{\tilde{\tau}_1}^2 > 0$. Since this angle is close to the region where the coupling to the Z^0 almost vanishes, no limit can be inferred from the LEP1 measurements, and the search was extended down to stau masses around 2 GeV/c^2. Stable or long lived particles with masses down to 2 GeV/c^2 are excluded by the search for heavy stable and long-lived particles in DELPHI [11]. Stable or long lived particles with masses below 2 GeV/c^2 are excluded by the JADE collaboration [31]. It is assumed that a stau with lower mass than a tau is stable or very long lived. In the case of short lived staus ($m_{\tilde{G}} \lesssim 0.03$ eV/c^2), a narrow band at $m_\tau < m_{\tilde{\tau}_1} < 2$ GeV/c^2 is not excluded. Above 2 GeV/c^2 the results from the impact parameter and secondary vertex analyses are used for exclusion purposes.

The impact parameter and secondary vertex analyses allow for the exclusion of $\tilde{\tau}_1$ ($\tilde{\tau}_R$) with a mass below 80 GeV/c^2 for gravitino masses between 10 and 310 eV/c^2 (8 and 380 eV/c^2) at 95% C.L.. For $m_{\tilde{G}}$ below a few eV/c^2, $m_{\tilde{\tau}_1} < 73$ GeV/c^2 were excluded by the search for $\tilde{\tau}_1$ in gravity mediated models [12]. Results from both searches were not combined because the impact parameter searches cover in excess the overlaping region. For $m_{\tilde{G}}$ larger than 1000 eV/c^2 the limit is 87 GeV/c^2, obtained after combining the results presented in this paper with those of the stable heavy lepton search [11].

Within the sleptons co-NLSP scenario, the cross-section limits of figures 8-b and -c were used to derive limits for $\tilde{\mu}_R$ (fig 12-a) and $\tilde{e}_R$ (fig. 12-b) masses at 95% C.L.. The $\tilde{\mu}_R$- pair production cross-section is model independent since it only takes place through the exchange of a Z^0 or a γ in the s–channel. The $\tilde{e}_R$- pair production cross-section, however, is a function of the GMSB parameters due to the exchange of a $\tilde{\chi}_1^0$ in the t–channel. Therefore, in order to put limits to the $\tilde{e}_R$ mass, the aforementioned region of the GMSB parameter space was scanned, and for each selectron mass the smallest theoretical production cross-section was chosen for comparison with the experimental limits.

The t-channel interference causes a bigger fraction of selectrons to be produced in the forward region. This results in a loss of efficiency in the vertex and stable slepton analyses, that was taken into acount for the calculation of the limits that are shown in fig. 12-b.

Therefore, within the co-NLSP scenario, the impact parameter search and the secondary vertex search allow for the exclusion of $\tilde{\mu}_R$ masses below 80 GeV/c^2 for gravitino masses between 8 and 450 eV/c^2. In the case of $\tilde{e}_R$, masses below 67 GeV/c^2 for gravitino masses between 10 and 80 eV/c^2 are excluded.

Assuming mass degeneracy between the staus and smuons, (fig. 12-c), these searches exclude at 95% C.L. $\tilde{l}_R$ masses below 84 GeV/c^2 for $\tilde{G}$ masses between 9 and 570 eV/c^2. For very short lifetimes only $\tilde{\mu}_R$ was considered since it is the best limit that can be achieved in absence of slepton combination. For $\tilde{G}$ larger than 1000 eV/c^2 the limit was 87 GeV/c^2, obtained from the stable heavy lepton search [11]. $\tilde{l}_R$ masses below 35 GeV/c^2

are excluded from LEP 1 data [32]. In the case of $\tilde{l}_R$ degeneracy, this limit improves to 41 GeV/c^2.

4.4.3 Chargino pair production

The limits on chargino pair production cross-section were used to exclude areas within the $(m_{\tilde{\chi}_1^+}, m_{\tilde{\tau}_1})$ plane in different domains of the gravitino mass [4].

Figure 13 shows the regions excluded at 95% CL in the $(m_{\tilde{\chi}_1^+}, m_{\tilde{\tau}_1})$ plane. The positive-slope area is excluded for all gravitino masses. The negative-slope area is only excluded for $m_{\tilde{G}} \geq 100$ eV/c^2. The area below $m_{\tilde{\tau}_1} = 75.8$ GeV/c^2 is excluded by the direct search for stau pair production [12]. The area of $\Delta m \leq 0.3$ GeV/c^2 is not excluded because in this regions the charginos do not decay mainly in $\tilde{\tau}_1$ and ν_τ, but in W and $\tilde{G}$. Thus, if $\Delta m \geq 0.3$ GeV/c^2, limits at 91.8, 93.0 and 93.0 GeV/c^2 can be set for $m_{\tilde{G}} = 1$, 100 and 1000 eV/c^2 respectively. The limit at $m_{\tilde{G}} = 1$ eV/c^2 is also valid for smaller masses of the gravitino, because they lead to the same final state topologies. The same argument is true for $m_{\tilde{G}} \geq 1$ keV/c^2. The chargino mass limit decreases with decreasing $m_{\tilde{\tau}_1}$ because in scenarios with gravitino LSP, small stau masses correspond to small sneutrino masses (both are proportional to Λ), and hence to smaller production cross-sections due to the destructive interference between the s- and t-channels. It should be noticed that within the parameter space that concerns this work, the lightest chargino is at least 40% heavier than the lightest neutralino. Thus, for small gravitino masses the search for neutralinos implies a lower limit on the lightest chargino of 120 GeV/c^2. Neutralinos are not directly searched for in heavier gravitino mass regions and therefore the limit of 93 GeV/c^2 remains valid.

4.4.4 Limits on the GMSB parameter space

Finally, all these results can be combined to produce exclusion plots within the $(\tan\beta, \Lambda)$ space. As an example, fig. 14 shows the zones excluded for $n = 1$ to 4 for $m_{\tilde{G}} \leq 1$ eV/c^2, which corresponds to the NLSP decaying at the main vertex. The shaded areas are excluded. The areas below the dashed lines contain points of the GMSB parameter space with $\tilde{\chi}_1^0$-NLSP. The areas to the right (above for $n = 1$) of the dashed-dotted lines contain points of the GMSB parameter space where sleptons are the NLSP. It can be seen that the region of slepton-NLSP increases with n. The contrary occurs to the region of neutralino-NLSP. A limit can be set for the variable Λ at 16.5 TeV.

5 Summary

Lightest neutralino-, slepton- and chargino pair production were searched for in the context of light gravitino scenarios. Two scenarios were explored: the $\tilde{\tau}_1$ NLSP and the $\tilde{l}_R$ co-NLSP scenarios. No evidence for signal production was found. Hence, the DELPHI collaboration sets lower limits at 95% C.L. for the mass of the $\tilde{\chi}_1^0$ at 82 GeV/c^2 if $m_{\tilde{G}} \leq 1$ eV/c^2, for the mass of the $\tilde{\tau}_1$ at 73 GeV/c^2, the $\tilde{l}_R$ at 79 GeV/c^2, and the lightest chargino at 93 GeV/c^2 for all $m_{\tilde{G}}$. A limit is also set on the variable Λ at 16.5 TeV if $m_{\tilde{G}} \leq 1$ eV/c^2.

Acknowledgements

References

[1] M. Dine, W. Fischler and M. Srednicki, Nucl. Phys. **B189** (1981) 575 ;
S. Dimopoulos and S. Raby, Nucl. Phys. **B192** (1981) 353 ;
M. Dine and W. Fischler, Phys. Lett. **B110** (1982) 227 ;
M. Dine and M. Srednicki, Nucl. Phys. **B202** (1982) 238 ;
L. Alvarez-Gaumé, M. Claudson and M. Wise, Nucl. Phys. **B207** (1982) 96 ;
C. Nappi and B. Ovrut, Phys. Lett. **B113** (1982) 175 .

[2] M. Dine and W. Fischler, Nucl. Phys. **B204** (1982) 346 ;
S. Dimopoulos and S. Raby, Nucl. Phys. **B219** (1983) 479.

[3] J. A. Bagger, K. Matchev, D. M. Pierce and R. Zhang, Phys. Rev. **D55** (1997) 3188.

[4] D. A. Dicus, B. Dutta, S. Nandi, Phys. Rev. **D56** (1997) 5748 ;
D. A. Dicus, B. Dutta, S. Nandi, Phys. Rev. Lett. **78** (1997) 3055 ;
K. Cheung, D. A. Dicus, B. Dutta, S. Nandi, Phys. Rev. **D58** (1998) 015008 .

[5] F. Borzumati, *On the Minimal Messenger Model*, hep-ph/9702307 and WIS/96-50-PH, Dec. 1996.

[6] G. F. Giudice, R. Rattazzi, Phys. Rep. 322 (1999) 419..

[7] A. Bartl *et. al.*, Z. Phys. **C73** (1997) 469.

[8] S. Dimopoulos, M. Dine, S. Raby, S. Thomas and J. D. Wells, Nucl. Phys. Proc. Suppl. **A52** (1997) 38.

[9] E. Calzetta, A. Kandus, F. D. Mazzitelli and C. E. M. Wagner, CERN-TH/99-261 and hep-ph/9908524.

[10] DELPHI Collaboration, P. Abreu *et al.*, E. Phys.J. **C7** (1999) 595.

[11] DELPHI Collaboration, P. Abreu *et al.*, Phys. Lett. **B444** (1998) 491;
DELPHI Collaboration, P. Abreu *et al.*, CERN-EP-2000-020 accepted by Phys. Lett. **B**.

[12] DELPHI Collaboration, P. Abreu *et al.*, "Searches for sleptons at $\sqrt{s} = 183$ and 189 GeV", to be submitted to Phys. Lett. **B**.

[13] DELPHI Collaboration, P. Abreu *et al.*, Phys. Lett. **B466** (1999) 61.

[14] DELPHI Collaboration, P. Aarnio *et al.*, Nucl. Instr. and Meth. **303** (1991) 233.

[15] DELPHI Collaboration, P. Abreu *et al.*, Nucl. Instr. and Meth. **378** (1996) 57.

[16] T. Sjöstrand, Comp. Phys. Comm. **39** (1986) 347;
T. Sjöstrand, PYTHIA 5.6 *and* JETSET 7.3, CERN-TH/6488-92.

[17] DELPHI Collaboration, P. Abreu *et al.*, Z. Phys. **C73** (1996) 11.

[18] SUSYGEN 2.20, S. Katsanevas and S. Melachroinos in *Physics at LEP2*, CERN 96-01, Vol. 2, p. 328 and http://lyoinfo.in2p3.fr/susygen/susygen.html ;
S. Katsanevas and P. Moravitz, Comp. Phys. Com. 122 (1998) 227.

[19] DELPHI Collaboration, P. Abreu *et al.*, Phys. Lett. **B446** (1999) 75.

[20] DELPHI Collaboration, P. Abreu *et al.*, CERN-EP-2000-008, accepted by Phys. Lett. **B**.

[21] J.E. Campagne and R. Zitoun, Z. Phys. **C43** (1989) 469.

[22] S. Jadach, B.F.L. Ward and Z. Was, Comp. Phys. Comm. **79** (1994) 503.

[23] F.A. Berends, R. Kleiss, W. Hollik, Nucl. Phys. **B304** (1988) 712.

[24] F.A. Berends, R. Pittau, R. Kleiss, Comp. Phys. Comm. **85** (1995) 437.

[25] S. Nova, A. Olshevski, and T. Todorov, *A Monte Carlo event generator for two photon physics*, DELPHI note 90-35 (1990).

[26] F.A. Berends, P.H. Daverveldt, R. Kleiss, Comp. Phys. Comm. **40** (1986) 271, Comp. Phys. Comm. **40** (1986) 285, Comp. Phys. Comm. **40** (1986) 309.

[27] DELPHI Collaboration, P. Abreu *et al.*, Eur. Phys. J. **C6** (1999) 385.

[28] V. Barger *et al.*, Phys. Rev. D53 (1996)6407.

[29] A.L. Read, *Optimal statistical analysis of search results based on the likelihood ratio and its application to the search for the MSM Higgs boson at $\sqrt{s} = 161$ and 172 GeV*, DELPHI 97-158 PHYS 737 (1997) and references therein.

[30] DELPHI Collaboration, P. Abreu *et al.*, Eur. Phys. J.**C6** (1999) 371;
DELPHI Collaboration, P. Abreu *et al.*, "Photons events with missing energy at LEP 2", CERN-EP-2000-021, submitted to Eur. Phys. J. **C**.

[31] JADE Collaboration, W. Bartel *et al.*, Phys. Lett. B152 (1985) 392.

[32] Particle Data Group, Eur. Phys. J. **C3** (1998) 1.

Cut	$\gamma\gamma$	$ff\gamma$	4-fermion	Total MC	Data	Signal
pre-selection	1134 ± 37	413 ± 14	385 ± 18	1933 ± 43	1791	59.5%
1	28 ± 3	330 ± 11	363 ± 18	721.3 ± 21	706	51.2%
2	4.3 ± 1.2	11.1 ± 1.5	12.5 ± 2.8	28.0 ± 3.4	24	42.1%
3	0	0.07 ± 0.07	1.13 ± 0.3	1.2 ± 0.3	2	32.8%

Table 1: Number of events remaining in the data and simulated samples at $\sqrt{s} = 189$ GeV after the various stages of the selection procedure described in the search for neutralinos decaying into slepton and lepton. The signal efficiencies corresponds to $m_{\tilde{\chi}_1^0} = 87$ GeV/c^2 and $m_{\tilde{l}} = 75$ GeV/c^2.

Cut	$\gamma\gamma$	$ff\gamma$	4-fermion	Total MC	Data	Signal
pre-selection	1134 ± 37	413 ± 14	385 ± 18	1933 ± 43	1791	57.7%
1	66.5 ± 7	376.4 ± 13.0	331.0 ± 12.1	468.5 ± 19.1	404	54.5%
2	6.7 ± 1.8	9.5 ± 1.3	10.6 ± 0.9	26.8 ± 2.4	23	44.9%
3	0	0.07 ± 0.07	1.09 ± 0.3	1.16 ± 0.3	1	37.3%

Table 2: Number of events remaining in the data and simulated samples at $\sqrt{s} = 189$ GeV after the various stages of the selection procedure described in the search for neutralinos decaying into stau and tau. The signal efficiencies corresponds to $m_{\tilde{\chi}_1^0} = 87$ GeV/c^2 and $m_{\tilde{\tau}_1} = 75$ GeV/c^2.

Observed events	1
Total background	$1.42^{+0.72}_{-0.36}$
$Z^*/\gamma \to (ll)(n\gamma)$	$0.23^{+0.35}_{-0.01}$
4-fermion (except $\gamma\gamma$)	0.45 ± 0.16
$\gamma\gamma \to \tau^+\tau^-$	$0.74^{+0.59}_{-0.32}$

Table 3: Number of observed events at $\sqrt{s} = 189$ GeV, together with the total number of expected background events and the expected numbers from the individual background sources, for both large impact parameter and secondary vertex searches combined.

Observed events	4
Total background	$4.54^{+1.12}_{-0.57}$
$Z^*/\gamma \to (\tau\tau)(n\gamma)$	$1.33^{+0.46}_{-0.35}$
$\gamma\gamma \to \tau^+\tau^-$	$0.61^{+0.99}_{-0.38}$
WW	$2.52^{+0.26}_{-0.23}$
ZZ	$0.08^{+0.04}_{-0.03}$

Table 4: Expected simulated SM background events and selected data events at 189 GeV centre-of-mass energy for the small impact parameter search.

Sample	Efficiencies (%)	Main backgrounds	Expected b.g.	Observed events
$m_{\tilde{G}} = 1$ eV/c^2	24 - 36	WW , $\gamma\gamma$	38.9±4.9	36
$m_{\tilde{G}} = 100$ eV/c^2	28 - 50	$\gamma\gamma$	2.1±0.9	1
$m_{\tilde{G}} = 1000$ eV/c^2	0 - 63	$\mu\mu(\gamma)$	1.7±0.3	1

Table 5: Range of efficiencies for the different sets of chargino signals described in section 2, main sources of background, expected background and observed data events for the different analyses.

n	co-NLSP(GeV/c^2)	$\tilde{\tau}_1$-NLSP (GeV/c^2)
1	83.0	82.5
2	85.0	85.0
3	86.0	86.0
4	87.0	87.0

Table 6: The 95% C.L. lower limits on $m_{\tilde{\chi}_1^0}$ within the $\tilde{\tau}_1$-NLSP and co-NLSP scenarios for different n.
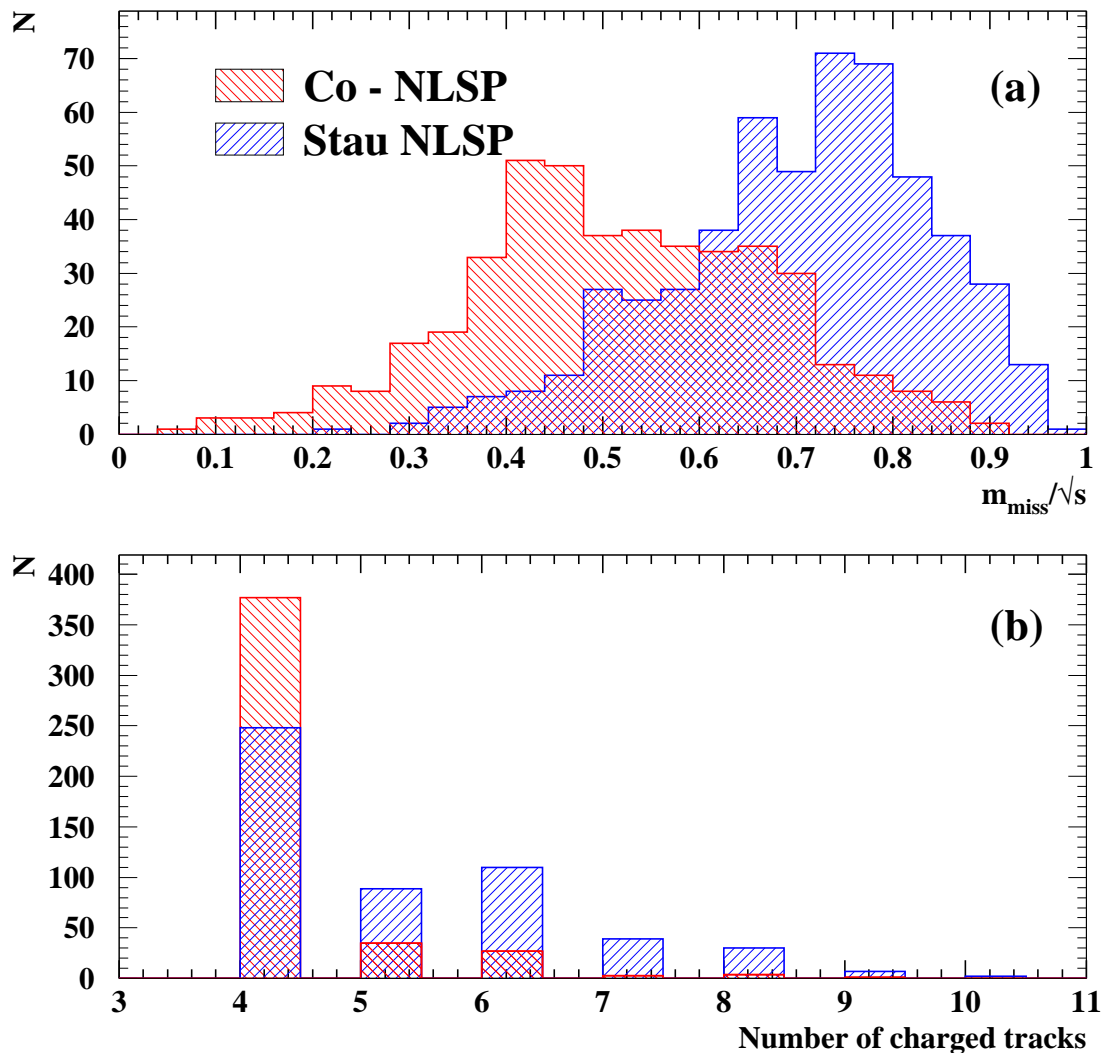
Figure 1: Two examples of kinematic differences between the $\tilde{\tau}_1$-NLSP and co-NLSP scenarios. Fig. (a) shows the distribution of the missing mass normalized to the centre-of-mass energy $(m_{miss}/\sqrt{s})$ for simulated sets with same mass neutralinos and same mass $\tilde{\tau}_1$ and slepton. Fig. (b) shows the number of charged tracks per event for the same two sets of simulated signals. Histograms with positive-slope shading show a set of $m_{\tilde{\chi}_1^0} = 82$ GeV/c^2 and $m_{\tilde{\tau}_1} = 80$ GeV/c^2. Histograms with negative-slope shading show a set of $m_{\tilde{\chi}_1^0} = 82$ GeV/c^2 and $m_{\tilde{l}_R} = 80$ GeV/c^2.
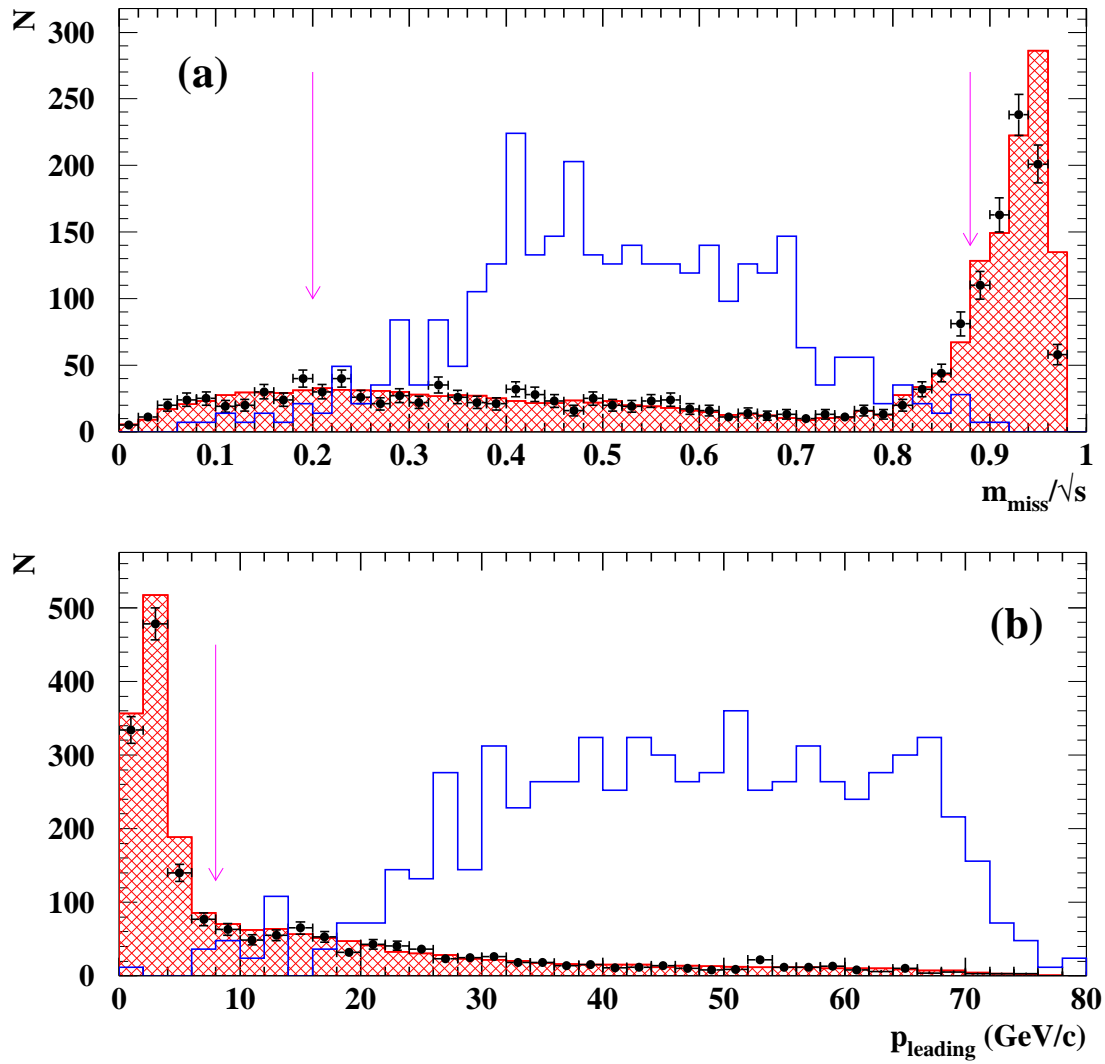
Figure 2: (a) Normalized missing mass and (b) momentum of the leading charged particle, for data (dots), Standard Model simulation (cross-hatched histogram) and one of the simulated signals with cross-section with arbitrary normalization (blank histogram) after preselection. The arrows indicate selection criteria imposed as explained in the text.
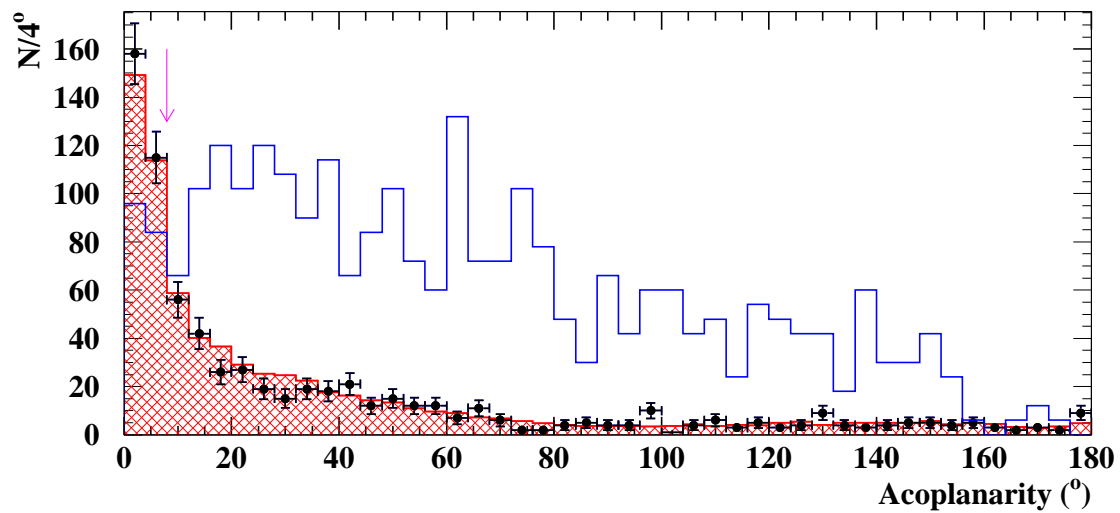
Figure 3: Acoplanarity of data (dots), Standard Model background simulation (cross-hatched histogram) and one of the simulated signals with cross-section not to scale (blank histogram), after the cut to remove $\gamma\gamma$ events. The arrow indicates selection criterion imposed as explained in the text.
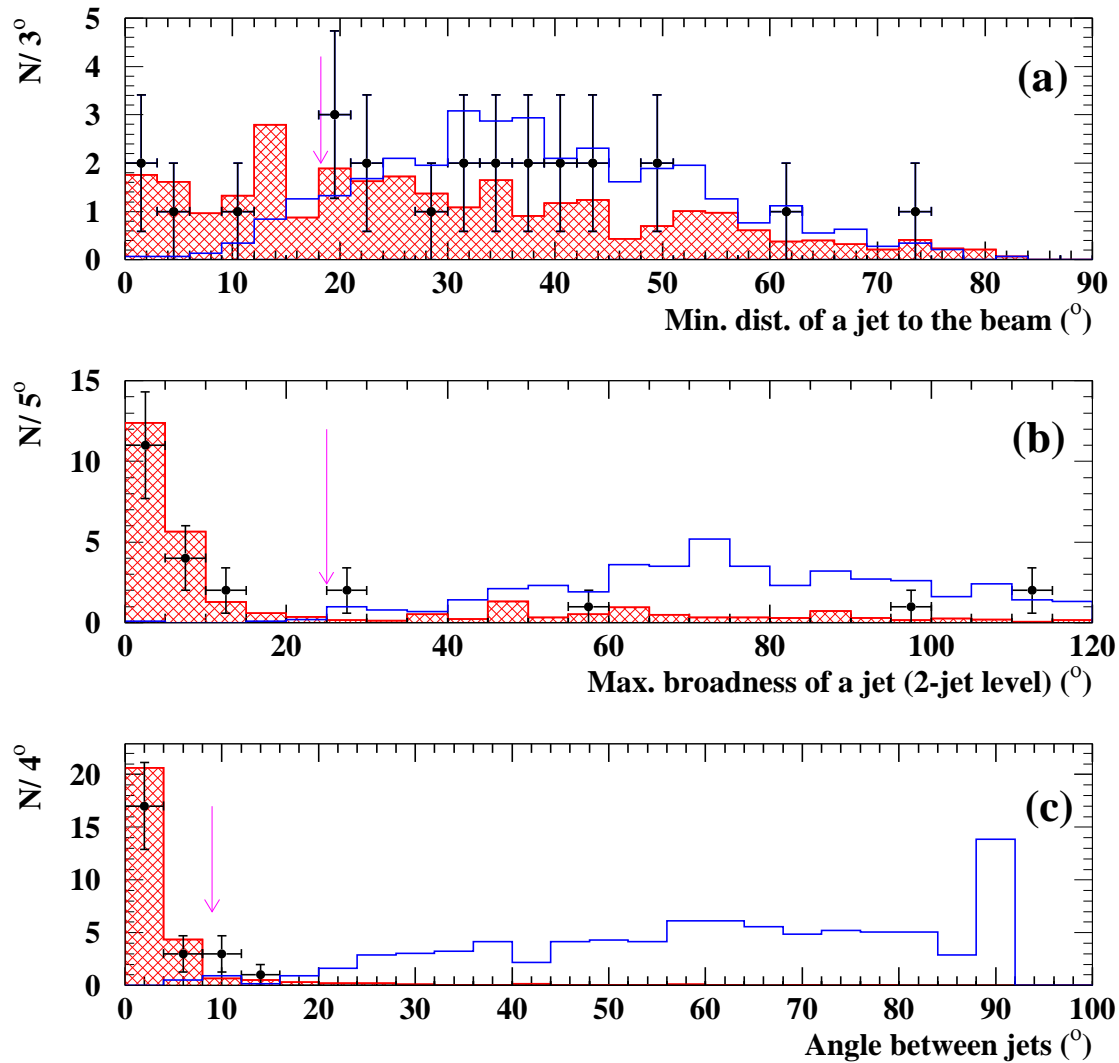
Figure 4: (a) Minimum angle of a jet to the beam, (b) maximum of angular broadness of the two jets at the 2-jet level and (c) minimum angle between jets at the 4-jet level, for data (dots), Standard Model background simulation (cross-hatched histogram) and one of the simulated signals with cross-section not to scale (blank histogram), after the cut to remove $f\bar{f}(\gamma)$ and 4-fermion events. The arrows indicate selection criteria imposed as explained in the text.
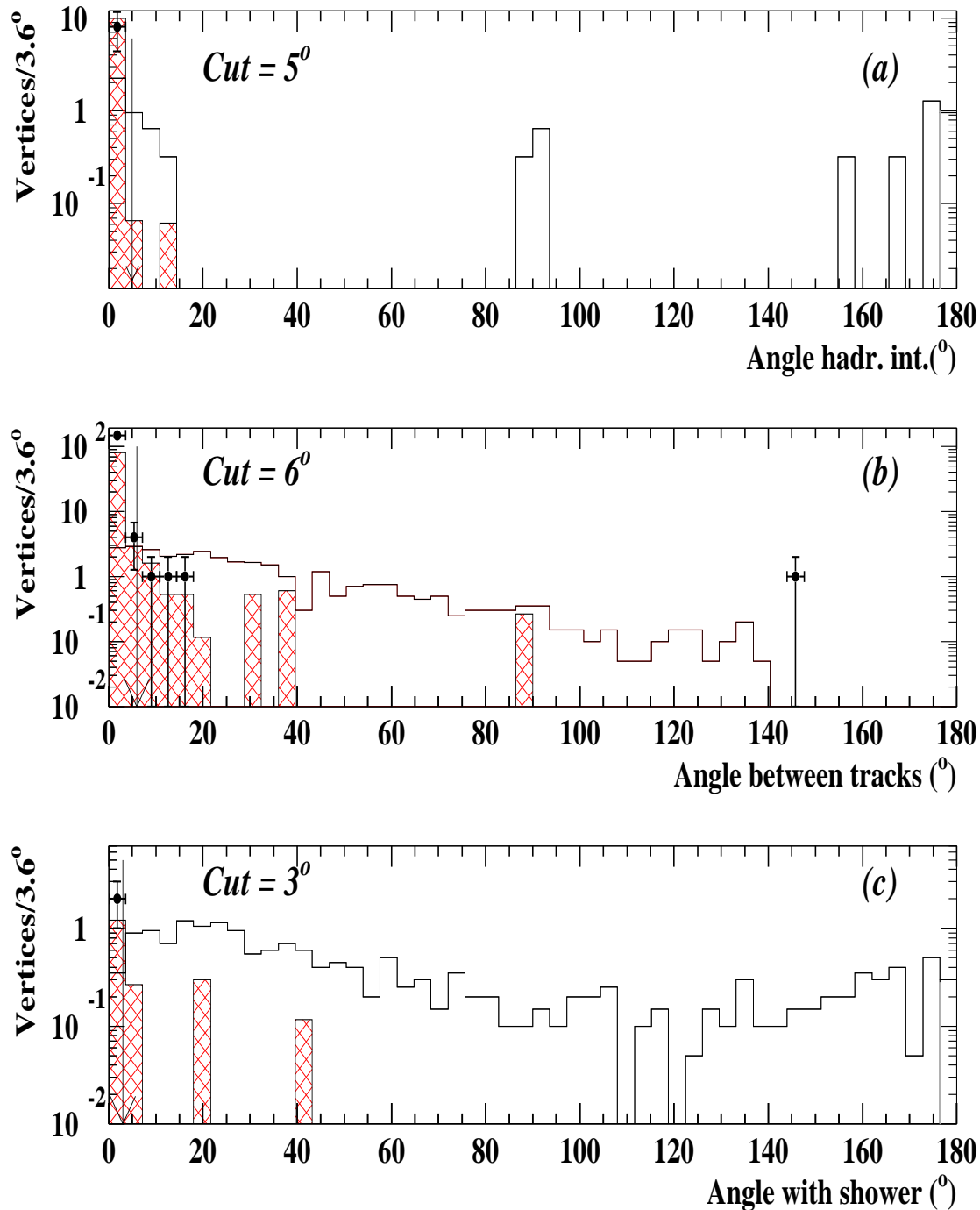
Figure 5: (a) Angle between the directions defined by the hadronic vertex and the reconstructed vertex, (b) angle between the tracks of the kink, and (c) angle between the electromagnetic shower and the direction defined by the difference between the momenta of the $\tilde{\tau}_1$ and its associated τ, defined at the crossing point for real data (dots), expected Standard Model background (cross-hatched histogram) and simulated signal for $m_{\tilde{\tau}_1} = 60$ GeV/c^2 decaying with a mean distance of 50 cm (blank histogram). Events that do not have hadronic interactions are not included in (a), and events without electromagnetic showers are not included in (b). The arrows indicate the selection criteria imposed.
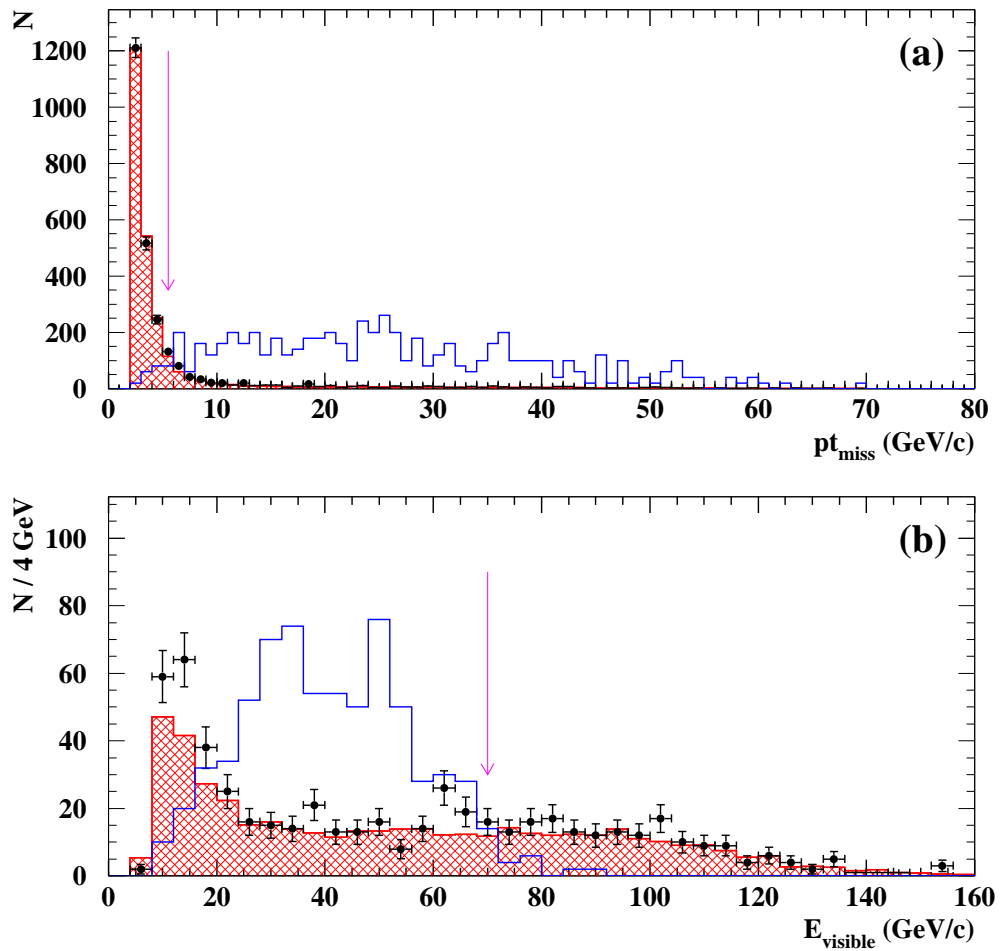
Figure 6: Missing transverse momentum (a) and visible energy (b), for real data (dots), expected Standard Model background (shaded histogram) and simulated signal for $m_{\tilde{\chi}_1^+} = 85$ GeV/c^2 and $m_{\tilde{\tau}_1^+} = 69$ GeV/c^2 decaying with a mean distance of 50 cm (blank histogram). The arrows indicate selection criteria imposed as explained in [19].
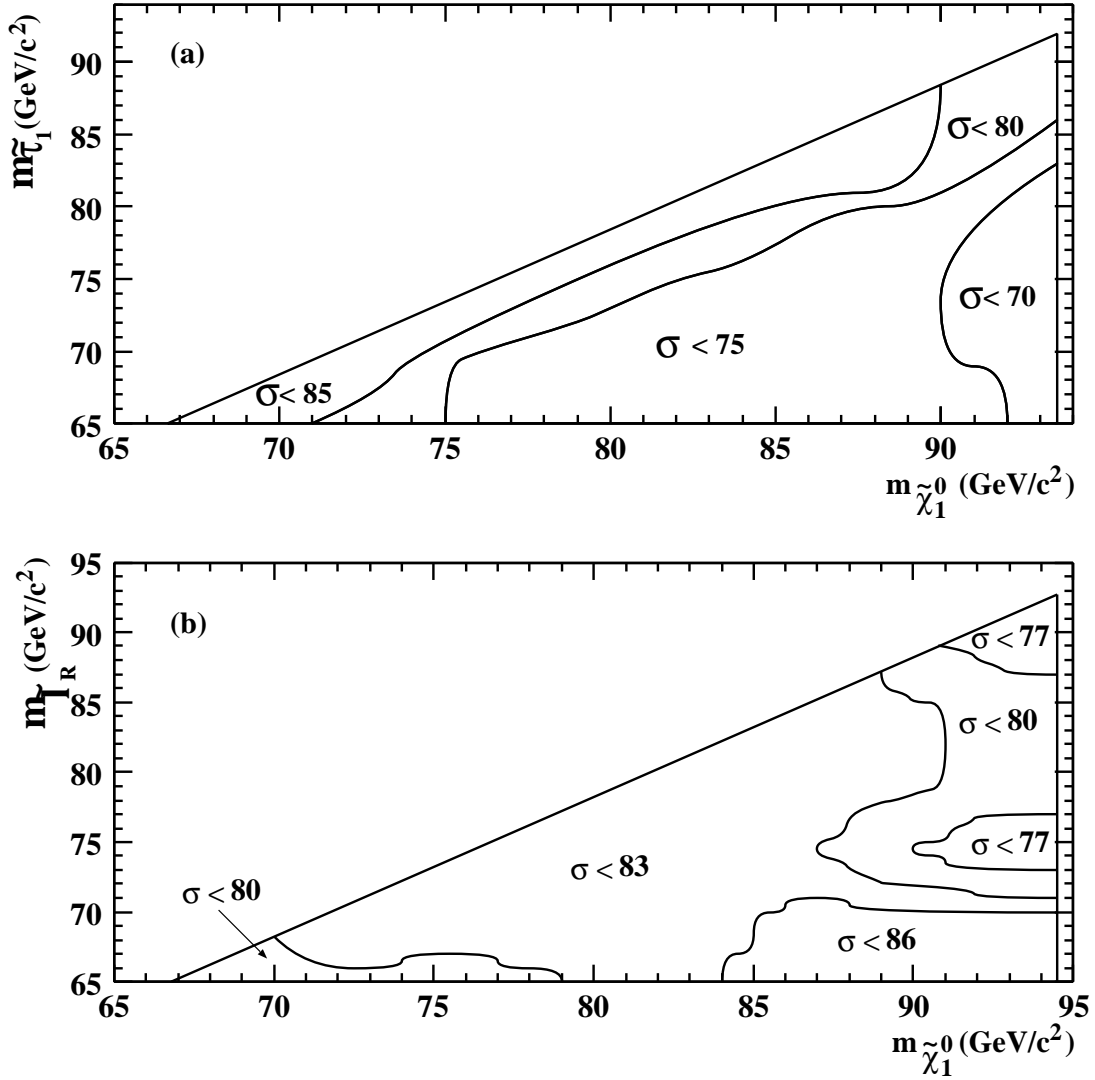
Figure 7: 95% C.L. upper limit of the $\tilde{\chi}_1^0$ pair production cross-section (in femtobarn) at $\sqrt{s} = 189$ GeV (a) after combining the results of the searches from $\sqrt{s} = 161$ up to 189 GeV, as a function of $m_{\tilde{\chi}_1^0}$ and $m_{\tilde{\tau}_1}$ for the case $n = 3$ in the $\tilde{\tau}_1$-NLSP scenario, where n is the number of messenger generations and (b) using data at $\sqrt{s} = 189$ GeV, as a function of $m_{\tilde{\chi}_1^0}$ and $m_{\tilde{l}_R}$ in the co-NLSP scenario. The diagonal and vertical lines show respectively the limits $m_{\tilde{\chi}_1^0} = m_{\tilde{\tau}} + m_{\tau}$ and $m_{\tilde{\chi}_1^0} = \sqrt{s}/2$.
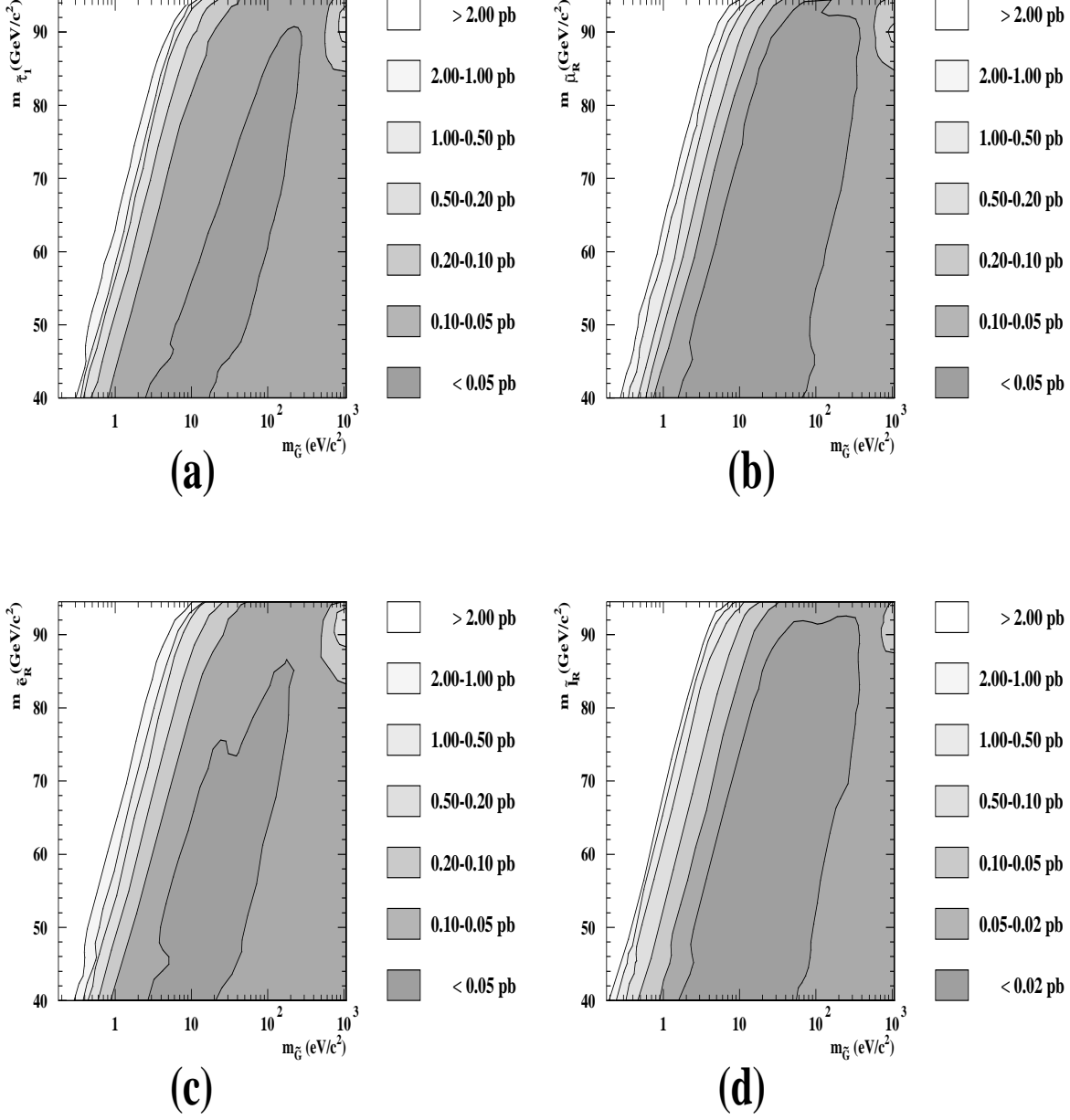
Figure 8: 95% C.L. upper limit of the $e^+e^- \to \tilde{\tau}_1\tilde{\tau}_1$ (a), $e^+e^- \to \tilde{\mu}_R\tilde{\mu}_R$ (b), $e^+e^- \to \tilde{e}_R\tilde{e}_R$ (c), and $e^+e^- \to \tilde{l}_R\tilde{l}_R$ (d) production cross-sections, at $\sqrt{s}$=189 GeV after combining the results of the searches at $\sqrt{s} = 130-189$ GeV. Results are shown in the $(m_{\tilde{G}},m_{\tilde{l}})$ plane. Searches for events containing charged particle tracks with small impact parameter, large impact parameter, secondary vertices and the search for heavy stable leptons are combined.
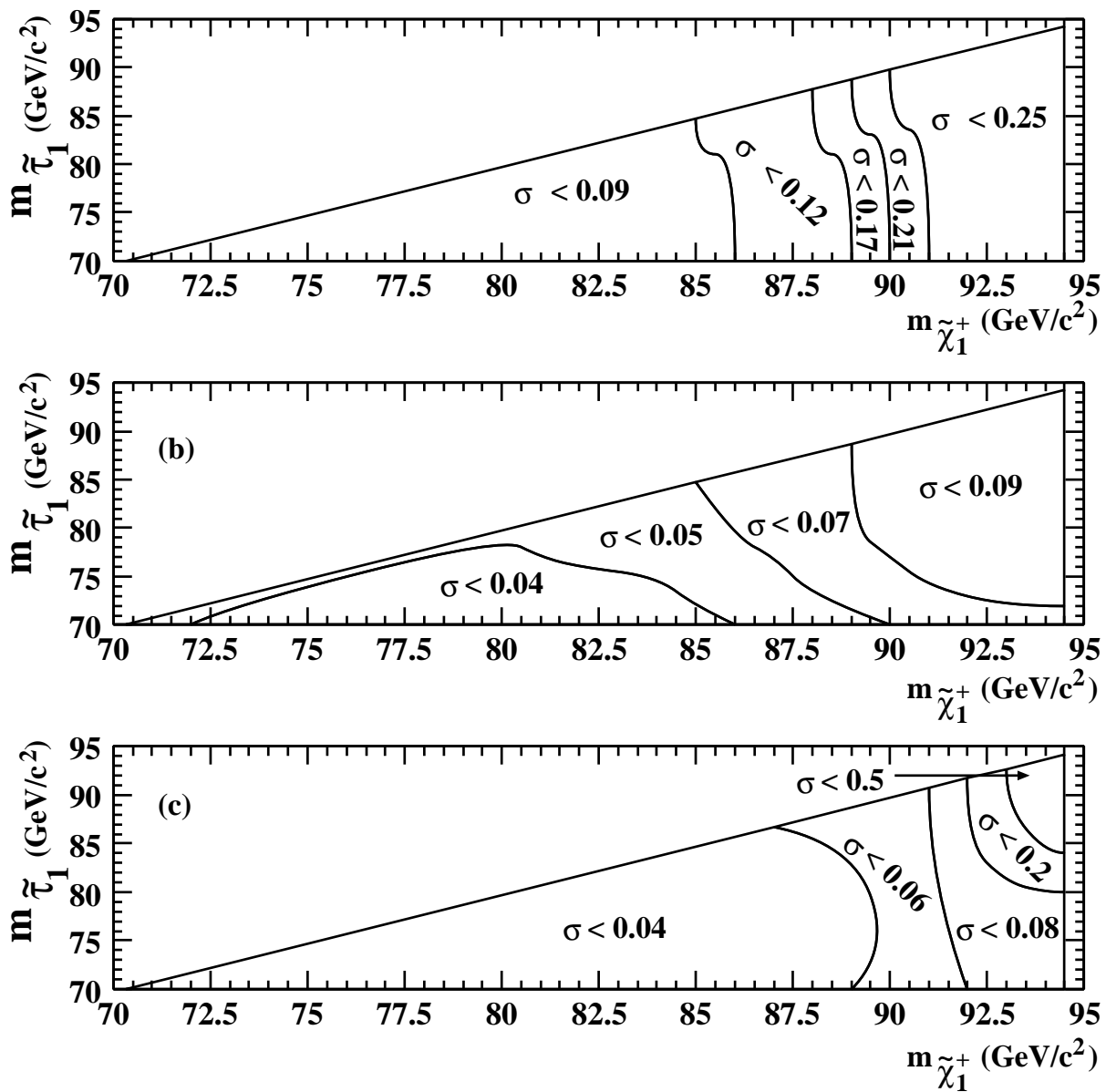
Figure 9: Limits in picobarn on the lightest chargino pair production cross-section at 95% CL. Limits are shown as functions of $m_{\tilde{\chi}_1^+}$ and $m_{\tilde{\tau}_1}$ for (a) $m_{\tilde{G}} = 1$ eV/c^2, (b) $m_{\tilde{G}} = 100$ eV/c^2 and (c) $m_{\tilde{G}} = 1000$ eV/c^2.
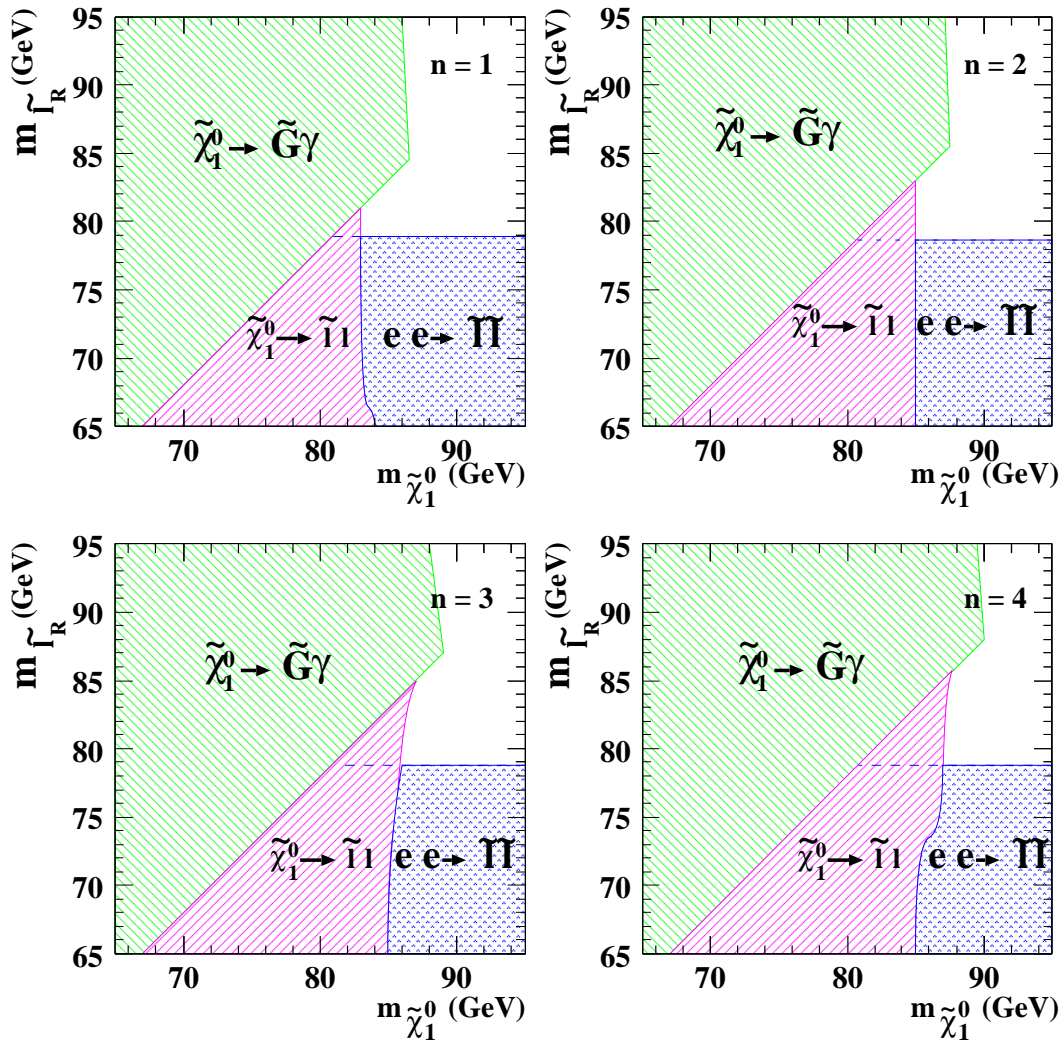
Figure 10: Areas excluded at 95% C.L. with $m_{\tilde{G}} < 1$ eV/c^2 in the $m_{\tilde{\chi}_1^0}$ vs. $m_{\tilde{l}_R}$ plane for $n = 1$ to 4. The positive-slope dashed area is excluded by this analysis. The negative-slope dashed area is excluded by the search for $\tilde{\chi}_1^0 \to \gamma\tilde{G}$, and the point-hatched area by the direct search for slepton pair production in the MSUGRA framework.
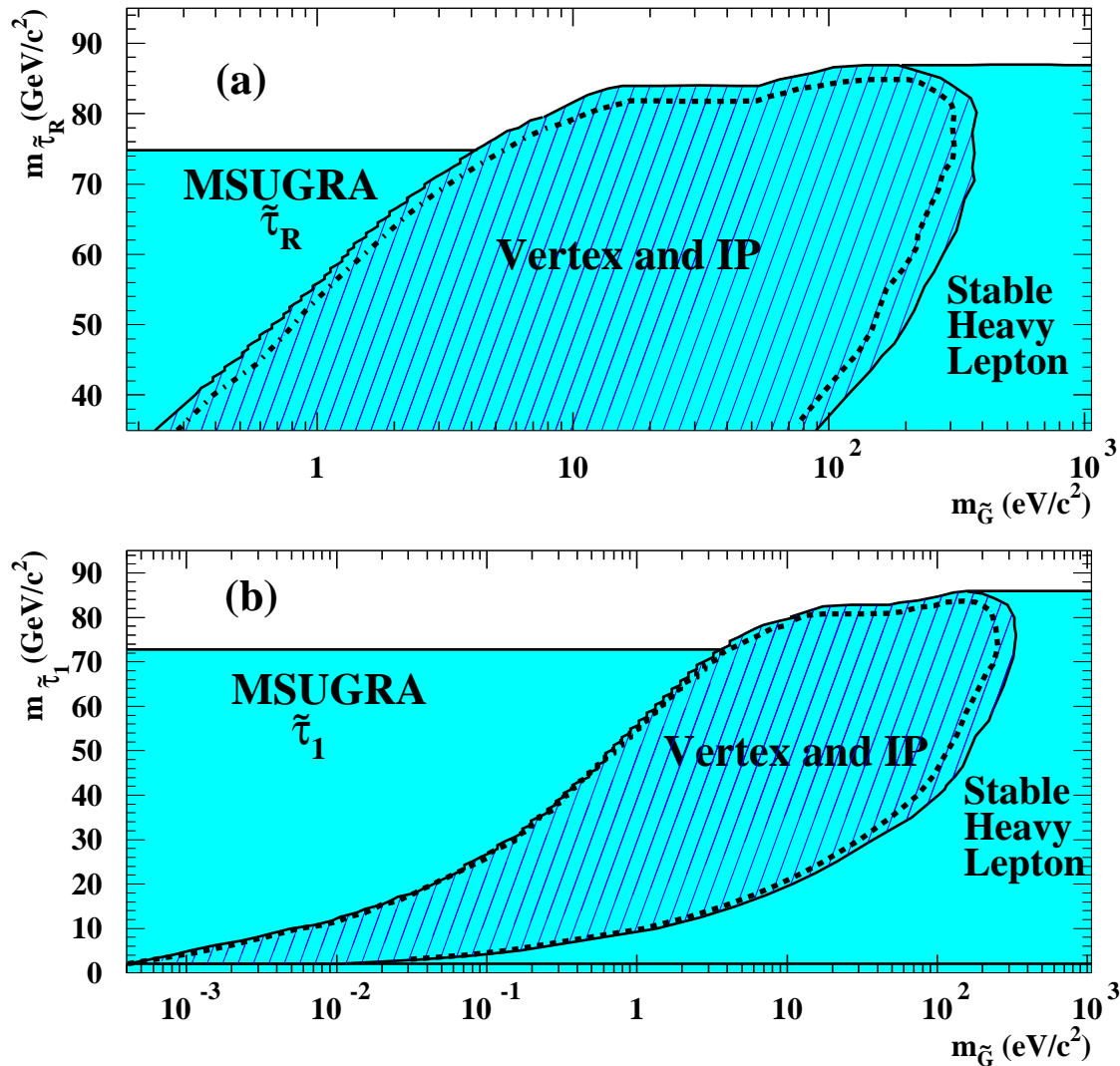
Figure 11: Exclusion region in the $(m_{\tilde{G}}, m_{\tilde{\tau}_R})$ plane (a) and $(m_{\tilde{G}}, m_{\tilde{\tau}_1})$ plane (b) at 95% C.L. for the present analysis combined with the stable heavy lepton search and the search for $\tilde{\tau}_1$ within MSUGRA models, using all LEP-2 data up to 189 GeV. The positive-slope hatched area shows the region excluded by the impact parameter and secondary vertex searches. The dashed line shows the expected limits. The area below the horizontal line in (b) is excluded by the JADE collaboration. A narrow band at $m_\tau < m_{\tilde{\tau}} < 2 \text{ GeV}/c^2$ and $m_{\tilde{G}} < 0.03 \text{ eV}/c^2$ is not excluded.
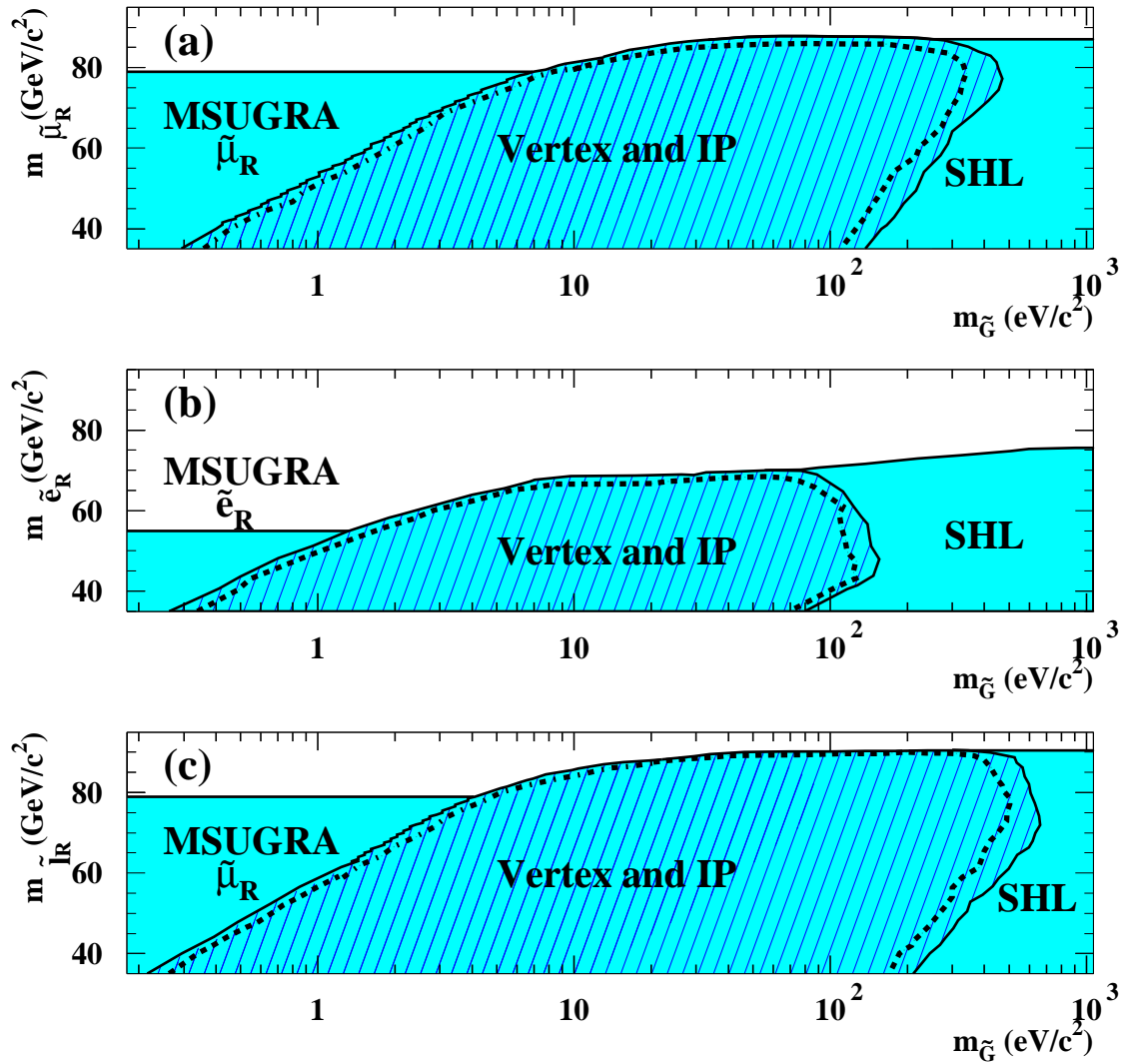
Figure 12: Exclusion regions in the $(m_{\tilde{G}}, m_{\tilde{\mu}_R})$ (a), $(m_{\tilde{G}}, m_{\tilde{e}_R})$ (b) and $(m_{\tilde{G}}, m_{\tilde{l}_R})$ (c) planes at 95% C.L. for the present analyses combined with the stable heavy lepton search and the search for $\tilde{\tau}_R$ in gravity mediated models, using all LEP2 data up to 189 GeV. The positive-slope hatched area shows the region excluded by the combination of the impact parameter and secondary vertex searches. The dashed line shows the expected limits.
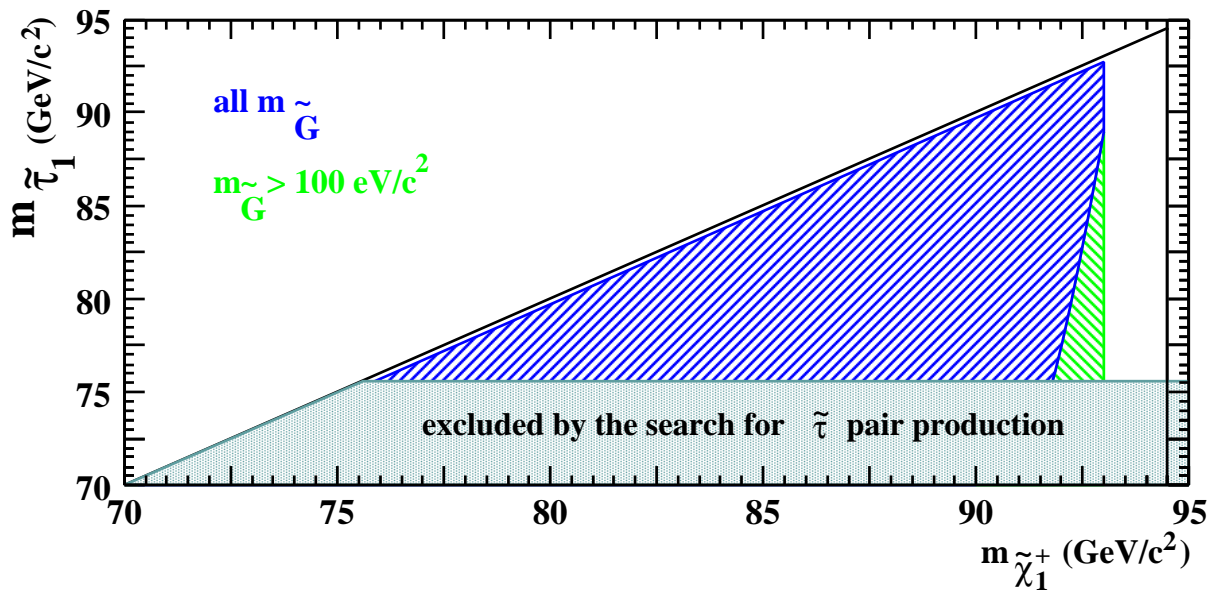
Figure 13: Areas excluded at 95% CL in the $(m_{\tilde{\chi}_1^+}, m_{\tilde{\tau}_1})$ plane. The positive-slope area is excluded for all $m_{\tilde{G}}$. The negative-slope area is excluded only for $m_{\tilde{G}} \geq 100$ eV/c^2. The grey area is excluded by the direct search for stau pair production [12].
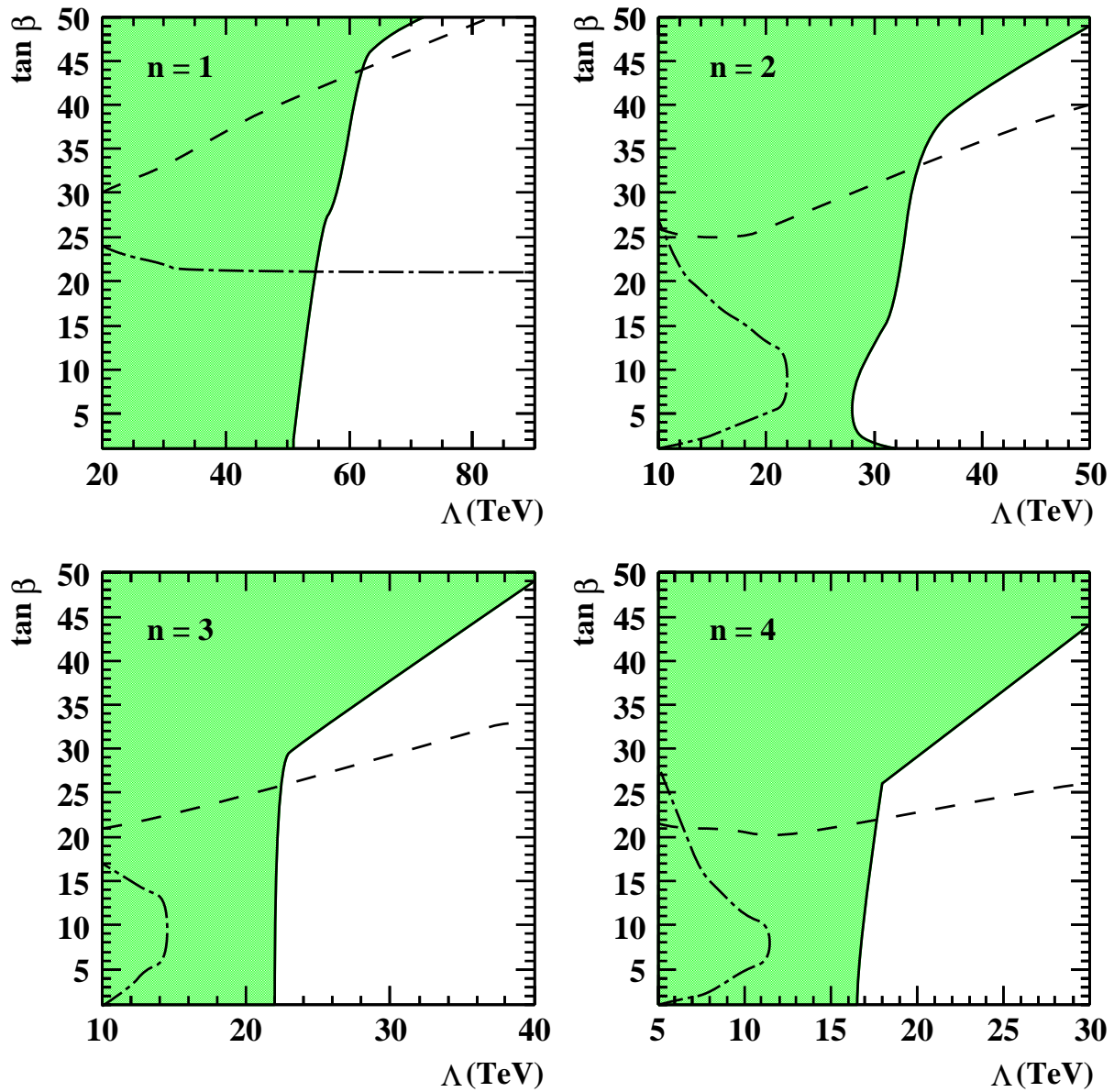
Figure 14: Shaded areas in the $(\tan\beta, \Lambda)$ plane are excluded at 95% CL. The areas below the dashed lines contain points of the GMSB parameter space with $\tilde{\chi}_1^0$-NLSP. The areas to the right (above for $n = 1$) of the dashed-dotted lines contain points of the GMSB parameter space were sleptons are the NLSP.